

# SYREN-NEW: Precise formulae for the linear and nonlinear matter power spectra with massive neutrinos and dynamical dark energy

Ce Sui <sup>\*1</sup>, Deaglan J. Bartlett <sup>\*\*2</sup>, Shivam Pandey<sup>3</sup>, Harry Desmond<sup>4</sup>, Pedro G. Ferreira<sup>5</sup>, and Benjamin D. Wandelt<sup>2,3,6,7</sup>

<sup>1</sup> Department of Astronomy, Tsinghua University, Beijing 100084, China.

<sup>2</sup> CNRS & Sorbonne Université, Institut d'Astrophysique de Paris (IAP), UMR 7095, 98 bis bd Arago, F-75014 Paris, France

<sup>3</sup> Department of Physics and Astronomy, Johns Hopkins University, Baltimore, MD 21218, USA

<sup>4</sup> Institute of Cosmology & Gravitation, University of Portsmouth, Dennis Sciama Building, Portsmouth, PO1 3FX, UK

<sup>5</sup> Astrophysics, University of Oxford, Keble Road, OX1 3RH, UK

<sup>6</sup> Department of Applied Mathematics and Statistics, Johns Hopkins University, Baltimore, MD 21218, USA

<sup>7</sup> Center for Computational Astrophysics, Flatiron Institute, 162 5th Avenue, New York, NY 10010, USA

Received XXX; accepted YYY

## ABSTRACT

*Context.* Current and future large scale structure surveys aim to constrain the neutrino mass and the equation of state of dark energy. To do this efficiently, rapid yet accurate evaluation of the matter power spectrum in the presence of these effects is essential.

*Aims.* We aim to construct accurate and interpretable symbolic approximations to the linear and nonlinear matter power spectra as a function of cosmological parameters in extended  $\Lambda$ CDM models which contain massive neutrinos and non-constant equations of state for dark energy. This constitutes an extension of the SYREN-HALOFIT emulators to incorporate these two effects, which we call SYREN-NEW (SYmbolic-Regression-ENhanced power spectrum emulator with NEutrinos and  $W_0 - w_a$ ). We also wish to obtain a simple approximation to the derived parameter  $\sigma_8$  as a function of the cosmological parameters for these models.

*Methods.* We utilise symbolic regression to efficiently search through candidate analytic expressions to approximate the various quantities of interest. Our results for the linear power spectrum are designed to emulate CLASS, whereas for the nonlinear case we aim to match the results of EUCLIDEMULATOR2. We compare our results to existing emulators and  $N$ -body simulations.

*Results.* Our analytic emulators for  $\sigma_8$ , the linear and nonlinear power spectra achieve root mean squared errors of 0.1%, 0.3% and 1.3%, respectively, across a wide range of cosmological parameters, redshifts and wavenumbers. The error on the nonlinear power spectrum is reduced by approximately a factor of 2 when considering observationally plausible dark energy models and neutrino masses. We verify that emulator-related discrepancies are subdominant compared to observational errors and other modelling uncertainties when computing shear power spectra for LSST-like surveys. Our expressions have similar accuracy to existing (numerical) emulators, but are at least an order of magnitude faster, both on a CPU and GPU.

*Conclusions.* Our work greatly improves the accuracy, speed and range of applicability of current symbolic approximations to the linear and nonlinear matter power spectra. These now cover the same range of cosmological models as many numerical emulators with similar accuracy, but are much faster and more interpretable. We provide publicly available code for all symbolic approximations found.

**Key words.** Cosmology: theory, Cosmology: cosmological parameters, Cosmology: large-scale structure of Universe, Cosmology: dark energy, Methods: numerical

## 1. Introduction

Despite the phenomenal successes of the standard models of cosmology ( $\Lambda$ CDM) and particle physics, we do not yet fully understand the nature of many of their constituents. In particular, it is known that the Universe is expanding and this expansion is accelerating, yet we do not know what the properties of the component of the Universe (dark energy) which drives this are. The current cosmological paradigm states that this is due to a cosmological constant, which has an equation of state which does not vary in time and is equal to -1, yet recent observations hint at deviations from these assumptions (DESI Collaboration et al. 2024). On smaller scales, we have, to date, detected three flavour eigenstates of neutrinos and oscillation experiments demonstrate that these can be mixed (e.g. Becker-Szendy et al. 1992; Fukuda

et al. 1998a,b; Ahmed et al. 2004). This implies that neutrinos must have non-zero mass. Although we can measure the differences between the neutrino masses with these techniques, the masses of the individual flavours remain unknown. We do not even know the order (hierarchy) of their masses, namely if it is “normal” ( $m_1 \leq m_2 \leq m_3$ , where  $m_i$  are the mass eigenstates and the smallest difference between the square of the masses is between  $m_1$  and  $m_2$ ) or “inverted” ( $m_3 \leq m_1 \leq m_2$ ).

One of the main aims of current and future large scale structure surveys such as *Euclid* (Laureijs et al. 2011), LSST (LSST Science Collaboration et al. 2009), DESI (DESI Collaboration et al. 2016) and the Nancy Grace Roman Space Telescope (Akeson et al. 2019) is to shed light on these fundamental questions. In particular, by studying their effects on cosmological scales (see, e.g. Lesgourgues & Pastor 2006; Weinberg et al. 2013), these experiments aim to constrain the equation of state of dark energy and the total mass of neutrinos.

\* suic20@mails.tsinghua.edu.cn

\*\* deaglan.bartlett@iap.fr

Central to current large scale structure analyses is the matter power spectrum; the Fourier transform of the two-point correlation function. By comparing the theoretical and observed power spectra, one can constrain cosmological parameters through techniques such as Markov Chain Monte Carlo. The matter power spectrum also serves as an input to the calculation of many other cosmological observables such as the shear power spectrum for weak lensing analyses or the galaxy power spectrum for clustering studies. In the absence of any accelerated modelling techniques, to compute the theoretical prediction down to very nonlinear scales accurately, one would have to run a new  $N$ -body simulation each time one updated the cosmological parameters. Or, even if one was only interested in relatively linear scales, one would still need to solve a complicated set of differential equations (Lewis et al. 2000; Blas et al. 2011; Hahn et al. 2024) to make this prediction. Given that these inferences require one to sample cosmological parameters many thousands of times, a significant amount of work has been dedicated to bypassing these requirements to significantly increase the speed of cosmological analyses.

Many of the techniques exploited to expedite these calculations involve the construction of “emulators”: typically advanced numerical machine learning based approaches (e.g. Gaussian Processes or Neural Networks) or interpolators designed to be used as surrogate models which directly output the power spectrum given a set of cosmological parameters. Some examples of these emulators are AEMULUS (Zhai et al. 2019), BACCO (Angulo et al. 2021; Aricò et al. 2021; Zennaro et al. 2023), COBRA (Bakx et al. 2024), COSMICEMU (Lawrence et al. 2017), COSMOPOWER (Spurio Mancini et al. 2022), DARK EMULATOR (Nishimichi et al. 2019), EMUPK (Mootoovaloo et al. 2022), EUCLIDEMULATOR1 (Euclid Collaboration et al. 2019), EUCLIDEMULATOR2 (Euclid Collaboration et al. 2021), FOFITTINGFUNCTION (Winther et al. 2019), FRANKENEMU (Heitmann et al. 2009, 2014), NGENHALOFIT (Smith & Angulo 2019), and PICO (Fendt & Wandelt 2007a,b). Although accurate to the percent level and considerably faster than the calculations which they are designed to replace, these have disadvantages particularly regarding interpretability. It is not clear how a given feature of the final prediction is sensitive to the input parameters, and it challenging to ensure that the emulated quantities have the correct asymptotic behaviour in well-known limits.

As an alternative, many symbolic approximations to the linear and nonlinear matter power spectra have been proposed. Arguably the most widely-used are the approximations by Eisenstein & Hu (1998, 1999), which give linear matter power spectra which are accurate to a few percent. These superseded the less accurate approximation by Bardeen et al. (1986) (BBKS) which did not include the effects of baryonic acoustic oscillations (BAOs). Analytic approximations to the nonlinear power spectrum have also been constructed, which rely on the halo model formalism (Ma & Fry 2000; Seljak 2000; Cooray & Sheth 2002). Assuming that matter in the Universe is bound in dark matter halos, one can either make this prediction by performing integrals of several quantities such as the halo density profile and mass function, as in the `HMCODE` approach (Mead et al. 2015, 2016, 2021), or one can adopt the `HALOFIT` method (Smith et al. 2003; Bird et al. 2012; Takahashi et al. 2012), where one directly predicts  $P(k)$  using an analytic function of the linear power spectrum and cosmological parameters.

These traditional symbolic approaches are not sufficiently accurate for modern applications, where percent-level predictions are required (Taylor et al. 2018). Hence, symbolic regression (SR; for a recent review see Kronberger et al. 2024) has

recently been employed as a method to improve these models by automatically and rapidly searching through candidate symbolic approximations to the matter power spectrum. Building off the approximation of Eisenstein & Hu (1998), Bartlett et al. (2024a) were able to obtain a symbolic emulator for the linear matter power spectrum of  $\Lambda$ CDM cosmologies which is accurate to 0.1% for  $k = 9 \times 10^{-3} - 9 h \text{Mpc}^{-1}$  and across a wide range of cosmological parameters. Similar work was performed by Orjuela-Quintana et al. (2024) who obtained an expression for the linear matter power spectrum in modified gravity models which has a typical accuracy of around 2% away from the BAOs, where the error is larger. The same authors extended their fit to include these features (Bayron Orjuela-Quintana et al. 2024) for universes with modified gravity and massive neutrinos, although this fit only achieves an accuracy of 3% in the power spectrum<sup>1</sup> near the first acoustic peak for the Planck 2018 cosmology (Planck Collaboration 2020), so does not meet the desired percent-level accuracy. To improve nonlinear predictions for the power spectrum, Bartlett et al. (2024b) introduced the `SYREN-HALOFIT` model: a SR-enhanced version of `HALOFIT` which is accurate to 1% for  $\Lambda$ CDM. Not only does this model have comparable accuracy to numerical emulators, but it was found to be between 36 and 950 times faster than alternative methods.

Given the desire to constrain deviations from  $\Lambda$ CDM in large scale structure studies, in this work we extend the work of Bartlett et al. (2024a,b) to obtain analytic approximations for the linear and nonlinear power spectra for cosmologies with non-zero neutrinos mass and a time-dependent equation of state for dark energy. We call this model `SYREN-NEW` (SYmbolic-Regression-ENhanced power spectrum emulator with NEutrinos and  $W_0 - w_a$ ). We base our linear power spectrum emulator on the approximation of Bartlett et al. (2024a), where we fit for the residuals between the predictions for the extended cosmology and that of  $\Lambda$ CDM. Unlike Bartlett et al. (2024b), for the nonlinear power spectrum, we do not fit corrections to existing `HALOFIT` formulae but allow SR to find a new, more accurate fitting formula without relying on previous expressions. As in Bartlett et al. (2024a), we also obtain a symbolic approximation to  $\sigma_8$  (a derived parameter) as a function of the other cosmological parameters. All our emulators achieve percent-level accuracy, making them comparably accurate to numerical approaches and to our previous approximations (Bartlett et al. 2024a,b). These expressions are not only interpretable, but have added advantages compared to their numerical counterparts; namely, they are faster to evaluate, more portable (they are easy to implement in the user’s favourite programming language) and potentially have better longevity (they do not become outdated when the underlying packages become deprecated since they only use standard mathematical operators).

The paper is organised as follows. In Section 2 we briefly introduce the matter power spectrum and discuss the cosmological models we are concerned with in this work. We then provide a short summary of SR in Section 3. Our emulators are constructed in the following three sections, with Section 4 detailing the approximation for  $\sigma_8$ , and Sections 5 and 6 describing the emulators for the linear and nonlinear power spectra, respectively. Our results are compared to pre-existing approximations and emulators in terms of speed and accuracy in Section 7, where we also study the correlation of our emulation errors with cosmo-

<sup>1</sup> The authors report an error of 1.5% on the transfer function at  $k \sim 0.1 h \text{Mpc}^{-1}$  for this cosmology. The power spectrum is proportional to the square of this quantity, hence the error on the power spectrum is twice as large as this value.

logical parameters and the impact on weak lensing studies when such errors are propagated through to shear power spectra. We conclude in Section 8. The main results of this paper are given in Eqs. (5), (28), (29) and (31) to (33). Throughout this paper “log” denotes the natural logarithm, and base-10 logarithms are denoted by “log<sub>10</sub>”.

## 2. Theoretical Background

Our goal is to develop an efficient, differentiable, and, if feasible, interpretable emulator for the power spectrum of matter fluctuations in the Universe, denoted as  $P(k, a, \theta)$ . Here,  $k$  represents the wavenumber,  $\theta$  stands for the cosmological parameters, and  $a$  is the scale factor ( $a = 1/(1+z)$  for redshift  $z$ ).

Separating the time-dependent matter density  $\rho(\mathbf{x}, a, \theta)$  in the Universe into a spatially constant background density,  $\bar{\rho}(a, \theta)$ , and a density contrast,  $\delta(\mathbf{x}, a, \theta)$ , such that  $\rho(\mathbf{x}, a, \theta) = \bar{\rho}(a, \theta)[1 + \delta(\mathbf{x}, a, \theta)]$ , the power spectrum is defined as follows. If  $\tilde{\delta}(\mathbf{k}, a, \theta)$  denotes the Fourier Transform of  $\delta(\mathbf{x}, a, \theta)$ , and the matter distribution is statistically homogeneous and isotropic, it follows that

$$(2\pi)^3 P(k, a, \theta) \delta^D(\mathbf{k} - \mathbf{k}') \equiv \langle \tilde{\delta}(\mathbf{k}, a, \theta) \tilde{\delta}^*(\mathbf{k}', a, \theta) \rangle, \quad (1)$$

where  $\langle \dots \rangle$  denotes an ensemble average and  $\delta^D$  is the Dirac delta function.

In this work we consider two versions of the matter power spectrum. For the “linear” power spectrum, which we denote as  $P_{\text{lin}}(k, a, \theta)$ , Eq. (1) is evaluated using  $\tilde{\delta}(\mathbf{k}, a, \theta)$  as computed using linear perturbation theory. The second variant uses the fully nonlinear value of  $\tilde{\delta}(\mathbf{k}, a, \theta)$  as is thus named the “nonlinear” power spectrum, and denoted by  $P_{\text{nl}}(k, a, \theta)$  in this paper.

Although much of the focus of this paper will be on obtaining symbolic approximations to  $P(k, a, \theta)$ , we will also find an emulator for  $\sigma_8$  as a function of the other cosmological parameters. This is defined using

$$\sigma_R^2 \equiv \int dk \frac{k^2}{2\pi^2} P_{\text{lin}}(k, a = 1, \theta) |W(k, R)|^2, \quad (2)$$

where the Fourier transfer of the top-hat filter is

$$W(k, R) = \frac{3}{(kR)^3} (\sin(kR) - kR \cos(kR)), \quad (3)$$

and  $\sigma_8$  is  $\sigma_R$  for  $R = 8h^{-1}\text{Mpc}$ . Performing such an integral can be time consuming, especially if one is, for example, post-processing a Markov Chain Monte Carlo analysis for which this is a derived parameter. Alternatively, if one required  $A_s$  for a given  $\sigma_8$ , the usual approach involves computing the linear matter power spectrum using a Boltzmann code with an initial estimate of  $A_s$ , then performing the integral in Eq. (2) to determine  $\sigma_8$ . For a desired  $\sigma_8$  value,  $\sigma'_8$ , one then uses  $A'_s = (\sigma'_8/\sigma_8)^2 A_s$ . Again, this can be time consuming.

This work considers an extended version of the  $\Lambda\text{CDM}$  model, described by the parameters given in Table 1. This model is an extension of  $\Lambda\text{CDM}$  in two ways. First, we study a Universe containing three massive neutrinos of equal mass, such that the sum of their masses is given by  $m_\nu$ , which is measured in eV throughout this work. Second, instead of assuming that dark energy is explained through a cosmological constant,  $\Lambda$ , we allow it to have a time-dependent equation of state. We adopt the commonly used Chevallier-Polarski-Linder (CPL) parameterisation (Chevallier & Polarski 2001; Linder 2003), such that

$$w(a) = w_0 + w_a(1 - a), \quad (4)$$

where  $\Lambda\text{CDM}$  corresponds to  $w_0 = -1$  and  $w_a = 0$ . Given the small dependence of the power spectrum on the reionisation optical depth parameter,  $\tau$ , we do not vary this in this work.

The ranges of the cosmological parameters given in Table 1 are almost identical to those given in Table 2 of Euclid Collaboration et al. (2021), except that we use a slightly smaller range of  $w_a$  ( $w_a < 0.5$  instead of  $w_a < 0.7$ ). Although Euclid Collaboration et al. (2021) state they allow these larger values of  $w_a$ , in fact they only train `EUCLIDEMULATOR2` on the same parameter range as Table 1, hence our emulators are trained on exactly the same range of cosmological models. Values of  $w_a$  larger than 0.5 give very different predictions than the rest of parameter space, since they allow models with  $w_0 + w_a = 0$ , and thus it is extremely challenging to obtain a single emulator covering all models if these values are included. Given that these models are not viable given current data (DESI Collaboration et al. 2024), this slight reduction of parameter space does not significantly weaken the applicability of our results.

In our previous papers (Bartlett et al. 2024a,b), we computed the linear power spectrum and  $\sigma_8$  using `CAMB` (Lewis et al. 2000). However, extending to  $w_0 - w_a$  is problematic since this involves some models for which  $w < -1$ , which is not permitted in `CAMB`. We therefore use `CLASS` (Blas et al. 2011) to compute the power spectrum variables of interest in this work since it can deal with these situations.

## 3. Symbolic regression

To derive analytical approximations for the linear and nonlinear power spectra and for  $\sigma_8$ , we utilise the supervised machine learning method of symbolic regression (SR) (Kronberger et al. 2024). In particular, we employ the widely-used genetic programming approach (Turing 1950; David 1989; Haupt & Haupt 2004). Genetic programming involves the evolution of “computer programs”, in our context, mathematical expressions represented as expression trees. Based on the principle of natural selection, at a given iteration, the least effective equations (as determined by a fitness metric) are eliminated, while new equations are generated through the combination of sub-expressions from the current population (crossover) or by randomly modifying subtrees within an expression (mutation). This process continues over numerous generations, gradually evolving the population of equations to produce increasingly accurate analytical expressions. We choose to use the SR package `OPERON`<sup>2</sup> (Burlacu et al. 2020) due to its speed, memory efficiency, and strong benchmark performance (Cava et al. 2021; Burlacu 2023). This code has been used successfully in many cosmological and astrophysical studies (Bartlett et al. 2024a,b; Russeil et al. 2024; AbdusSalam et al. 2024).

SR is typically viewed as a Pareto-optimisation problem, where one attempts to find accurate yet simple descriptions of the data. In our case, accuracy is determined by the root mean squared error between the predicted and target variable. To characterise simplicity, we use the “length” of the model. In `OPERON`, equations are encoded as trees, with each terminal node (e.g.,  $k$  or a cosmological parameter) being accompanied by a scaling parameter, which is then optimised (Kommenda et al. 2020) using the Levenberg–Marquardt algorithm (Levenberg 1944; Marquardt 1963). The “length” of an expression is defined to be the total number of nodes in the tree excluding the scaling terms.

During non-dominated sorting (NSGA2), `OPERON` utilises  $\epsilon$ -dominance (Laumanns et al. 2002), where  $\epsilon$  is defined such that

<sup>2</sup> <https://github.com/heal-research/operon>

**Table 1.** Cosmological parameters, redshifts and wavenumbers used for analytic emulators.

Parameter	Description	Minimum	Maximum
$10^9 A_s$	Spectral amplitude.	1.7	2.5
$\Omega_m$	Total matter (cold dark matter + baryons + neutrinos) density parameter.	0.24	0.40
$\Omega_b$	Baryonic density parameter.	0.04	0.06
$h$	Dimensionless Hubble parameter ( $H_0 = h \times 100 \text{ km s}^{-1} \text{ Mpc}^{-1}$ ).	0.61	0.73
$n_s$	Spectral index.	0.92	1.00
$w_0$	Time independent part of the dark energy equation of state (Eq. (4)).	-1.3	-0.7
$w_a$	Time dependent part of the dark energy equation of state (Eq. (4)).	-0.7	0.5
$m_\nu / \text{eV}$	Sum of neutrino mass (assuming three degenerate species).	0.00	0.15
$z$	Redshift.	0.0	3.0
$k / h \text{ Mpc}^{-1}$	Wavenumber.	$9 \times 10^{-3}$	9

**Notes.** All parameters are sampled independently and uniformly in the range between the minimum and maximum values given.

objective values (the accuracy and simplicity metrics) within  $\epsilon$  of each other are considered equal. This parameter impacts the number of duplicate equations in the population, promoting convergence to a well-distributed approximation of the global Pareto front: the set of solutions that cannot be improved in accuracy without increasing complexity. We experimented with different values for this parameter to determine settings that yield accurate yet compact models for our emulators, and we give the used values in the relevant sections for each one.

To select the best-fitting model, we first generate the Pareto front of candidate expressions. We then focus on models with a loss below a predetermined threshold (ensuring adequate accuracy for our purposes) and those with similar losses on training and validation sets (indicating minimal over-fitting). Although model selection can be automated (see, e.g. Bartlett et al. 2023, 2024; Cranmer et al. 2020), we opt to manually inspect the most accurate solution for each model length. This allows us to qualitatively select a function that is both sufficiently compact for interpretability and accurate enough for our needs.

#### 4. Analytic emulator for $\sigma_8$

We begin by examining the most basic emulator one might need for quantities related to the power spectrum: an emulator for  $\sigma_8$  as a function of other cosmological parameters, or equivalently, an emulator for  $A_s$  given  $\sigma_8$  and the remaining cosmological parameters. Our goal is to expedite Eq. (2) with a symbolic emulator. This is an extension of the emulator found by Bartlett et al. (2024a), who obtained a corresponding expression for  $\Lambda\text{CDM}$  which was accurate to 0.1%.

To find an emulator for our extended cosmology, we constructed a Latin hypercube (LH) sampling of 2000 sets of cosmological parameters, using uniform priors within the ranges specified in Table 1 (although we do not vary  $z$ , since we define  $\sigma_8$  at redshift zero). We created a second LH sampling of 2000 points for validation purposes. For these parameters, we computed  $\sigma_8$  using `CLASS` (Blas et al. 2011) and attempted to learn this mapping using a root mean squared error loss function with `OPERON`.

Given that the primordial power spectrum is proportional to the parameter  $A_s$ , through Eq. (2) one knows that  $\sigma_8 \propto \sqrt{A_s}$ . As such, following Bartlett et al. (2024a), instead of directly fitting for  $\sigma_8$ , we choose our target variable to be  $\sigma_8 / \sqrt{10^9 A_s}$ , which we fit for as a function of the other cosmological parameters. Using  $10^9 A_s$  instead of  $A_s$  enables the target variable to be  $\mathcal{O}(1)$ . Since we wish to find relatively compact expressions, we set the maximum model length to be 100. We found that a value of  $\epsilon =$

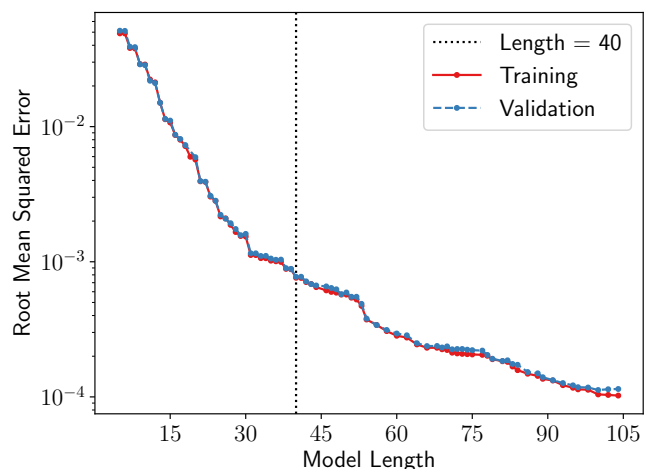


**Fig. 1.** Pareto front of solutions found by `OPERON` for  $\sigma_8 / \sqrt{10^9 A_s}$  as a function of cosmological parameters. We plot the curves for our training and validation sets separately, and indicate the chosen model (Eq. (5)) with a dotted vertical line.

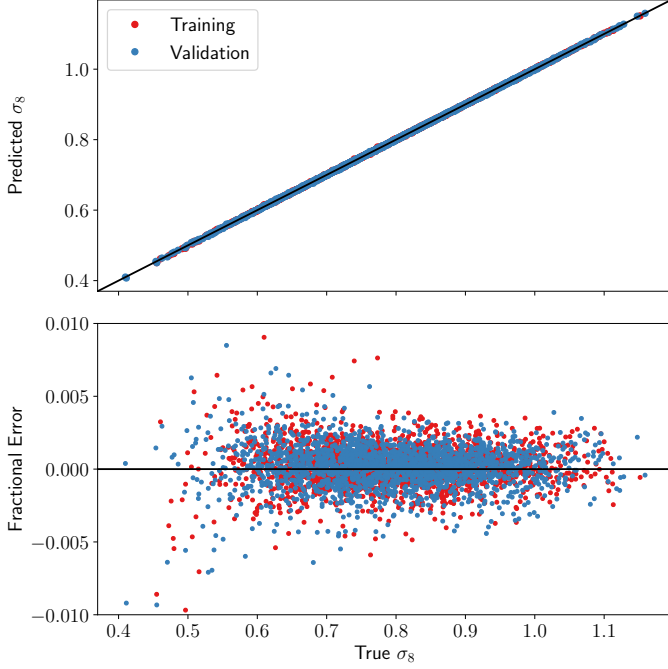
$10^{-3}$  was appropriate for this problem and allowed expressions to be formed of the operators  $+$ ,  $-$ ,  $\times$ ,  $\div$ ,  $\sqrt{\quad}$ , `pow` and `log`.

After searching for 1 hour with 56 cores, `OPERON` returned the Pareto front given in Fig. 1. We see that, for all model lengths, the training and validation losses are approximately equal, indicating that the models are not over-fitting. This is a particular advantage of SR, where the regularity on the solution space imposed by the requirement to use standard mathematical expressions makes over-fitting unlikely.

We observe that the error on the prediction decreases rapidly as one initially increases the model length, but this improvement becomes slower after a model length of approximately 30, where the root mean squared error is already at 0.1%. Given that we do not expect to require models which are much more accurate than this, to balance accuracy and simplicity, we choose to select a model from this region, although we note that more accurate models are achievable if one further increased the model length.

**Table 2.** Best-fit parameters for the  $\sigma_8$  emulator given in Eq. (5).

Param.	Value	Param.	Value	Param.	Value
$c_0$	0.0187	$c_6$	1.3057	$c_{12}$	-11.1463
$c_1$	-2.4891	$c_7$	0.0885	$c_{13}$	-1.5433
$c_2$	12.9495	$c_8$	0.1471	$c_{14}$	-7.0578
$c_3$	-0.7527	$c_9$	3.4982	$c_{15}$	2.0564
$c_4$	-2.3685	$c_{10}$	-0.006		
$c_5$	-1.5062	$c_{11}$	19.2779		

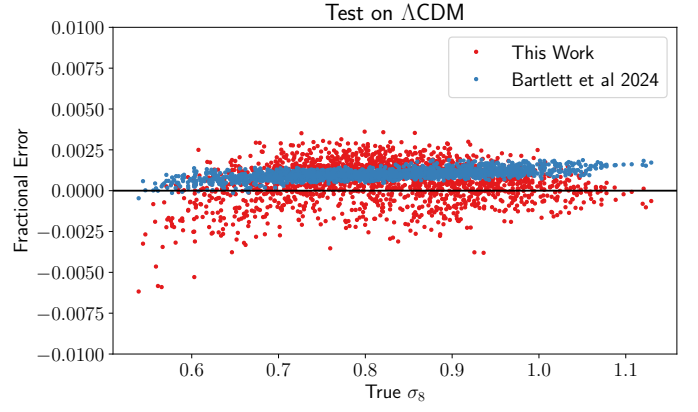

**Fig. 2.** Predicted values (upper) and fractional errors (lower) for the  $\sigma_8$  emulator (Eq. (5)) across the training and validation sets. The root mean squared error is 0.1%, with a maximum error of 1% for very small  $\sigma_8$  values.

As such, after inspecting these equations, we choose the model with length 40 as our fiducial result. This is given by

$$\begin{aligned} \frac{\sigma_8}{\sqrt{10^9 A_s}} \approx & c_0 (c_1 \Omega_b + c_2 \Omega_m + \log(c_3 w_0 + \log(c_4 w_0 + c_5 w_a))) \\ & \times (c_6 \Omega_m + c_7 m_\nu + c_8 n_s - \log(c_9 \Omega_m + c_{10} w_a)) \\ & \times (c_{11} \Omega_b + c_{12} \Omega_m - n_s) (c_{13} \Omega_m + c_{14} h + c_{15} m_\nu + n_s), \end{aligned} \quad (5)$$

with the parameters  $c$  given in Table 2. This expression achieves a root mean squared error on 0.1% on both the training and test sets. We give the most accurate expression we find in Appendix A, which has a root mean squared error of 0.02% on the validation set. We choose not to make this our fiducial model due since it is a long expression, although we encourage the user to use whichever model is preferable given their target accuracy.

To further investigate the performance of this emulator, in Fig. 2 we plot the predicted  $\sigma_8$  for each point on the training and validation LH as a function of the true value, and we also give the fractional error. We see that the fractional error on  $\sigma_8$  is approximately constant as the true values are varied, although for very small values of  $\sigma_8$  the error slightly increases to a maximum deviation of 1% at  $\sigma_8 \approx 0.5$ . These small values are incompatible with current observations (Planck Collaboration 2020), and thus


**Fig. 3.** Fractional error on the  $\sigma_8$  prediction for a test set which is restricted to  $\Lambda$ CDM models only. We compare the results of the emulator given here to that of Bartlett et al. (2024a). Our emulator has slightly weaker performance given its extended validity, but the error is almost always within 0.5%.

this small increase in error is unimportant for actual applications of this result.

Although we have produced this emulator for an extended cosmology, it is interesting to verify the performance on this emulator in the  $\Lambda$ CDM subspace to ensure that it can be applied to this situation. To do this, we generate a new LH of 2000 cosmologies within the  $\Lambda$ CDM portion of Table 1 and compute the corresponding  $\sigma_8$  values with CLASS. These are then compared against the predictions of Eq. (5) in Fig. 3, where we also show the results of using the emulator proposed in Bartlett et al. (2024a).

As one may expect, given that the emulator of Bartlett et al. (2024a) is specifically optimised for  $\Lambda$ CDM, whereas our method applies to a wider range of cosmologies, we obtain slightly larger emulation errors. We obtain almost identical root mean squared errors of approximately 0.1%, but the distribution of errors has slightly larger tails for this work compared to Bartlett et al. (2024a); our predictions remain almost always within 0.5%, whereas the Bartlett et al. (2024a) emulator has a maximum error of approximately 0.25%. We observe that Bartlett et al. (2024a) systematically overestimates the results. This is due to our use of CLASS instead of CAMB as the ground truth in this paper and since we included neutrino species in CLASS even when  $m_\nu = 0$ , which introduces slight deviations from the  $\Lambda$ CDM calculations used in Bartlett et al. (2024a) to obtain their result.

## 5. Analytic emulator for the linear power spectrum

We now consider the task of obtaining a symbolic approximation for the linear matter power spectrum. In the spirit of Bartlett et al. (2024a), rather than attempt to learn  $P_{\text{lin}}(k, a, \theta)$  in its entirety, we use some pre-existing approximations for the linear matter power spectrum, so that we only have to learn small corrections to these physics-informed formulae.

To incorporate previous approximations, we find that it is useful to write the linear matter power spectrum as

$$P_{\text{lin}}(k, a, \theta) = D_{\text{approx}}(k, a, \theta)^2 R(a, \theta) S(k, \theta) P_{\Lambda\text{CDM}}(k, \theta_{\Lambda\text{CDM}}), \quad (6)$$

where  $\theta$  contains all cosmological parameters, whereas  $\theta_{\Lambda\text{CDM}} = \{A_s, \Omega_m, \Omega_b, h, n_s\}$  are the subset of parameters describing

$\Lambda$ CDM. We will utilise existing results for two of these terms:  $D_{\text{approx}}$  (an approximation for the growth factor) and  $P_{\Lambda\text{CDM}}$  (an approximation for the  $\Lambda$ CDM linear power spectrum). We note that  $P_{\Lambda\text{CDM}}$  gives the shape of the linear matter power spectrum, which is equal to redshift-zero power spectrum up to some normalisation, which the other terms provide.

We therefore have to learn two terms which give corrections to this:

1.  $R(a, \theta)$ : This corresponds to (the square of) the correction to the linear growth factor approximation,  $D_{\text{approx}}$ .
2.  $S(k, \theta)$ : This is the correction to the redshift-zero linear power spectrum when moving from  $\Lambda$ CDM to the more general cosmological models.

These terms are defined such that  $R(a = 1, \theta) = 1 \forall \theta$ . Although one could make  $R$  depend on  $k$ , we found that the symbolic expressions we obtained when allowing for this dependence did not include  $k$ , and therefore we do not include this argument of the function.

We choose to fit for these corrections to  $\Lambda$ CDM rather than repeat the full fitting procedure of Bartlett et al. (2024a) given that we expect the shape of the baryonic acoustic oscillations to be independent of the neutrino mass and dark energy equation of state. Given that we already have a precise approximation to these in  $\Lambda$ CDM, it is simpler to fit the broad-band corrections to the shape of the power spectrum which should vary slowly in  $k$  and relatively smoothly in time.

In this section, we begin by describing the approximations we use from the literature to give  $D_{\text{approx}}$  (Section 5.1) and  $P_{\Lambda\text{CDM}}$  (Section 5.2). We then fit the correction terms to this in Section 5.3.

### 5.1. Approximation for the growth factor

To obtain the time-evolution of the linear matter power spectrum, we wish to have an approximation which we can correct with symbolic regression. Fortunately such an approximation already exists. We begin by defining the equality redshift as

$$z_{\text{eq}} = 2.5 \times 10^4 \Omega_{\text{m}} h^2 \Theta_{2.7}^{-4}. \quad (7)$$

Then, defining the time-dependent dark energy and dark matter density parameters as

$$\Omega_{\text{m}}(a) = \frac{\Omega_{\text{m}} a^{-3}}{\Omega_{\text{m}} a^{-3} + (1 - \Omega_{\text{m}}) a^{-3(1+w_0+w_a)} \exp(-w_a(1-a))}, \quad (8)$$

$$\Omega_{\Lambda}(a) = \frac{(1 - \Omega_{\text{m}}) a^{-3(1+w_0+w_a)} \exp(-w_a(1-a))}{\Omega_{\text{m}} a^{-3} + (1 - \Omega_{\text{m}}) a^{-3(1+w_0+w_a)} \exp(-w_a(1-a))}, \quad (9)$$

we use the following approximation for the growth factor in the absence of neutrinos (Lahav et al. 1991; Carroll et al. 1992; Eisenstein & Hu 1998)

$$D_1(a, \theta) = \frac{1 + z_{\text{eq}}}{1 + z} \frac{5\Omega_{\text{m}}(a)}{2} \left( \Omega_{\text{m}}(a)^{4/7} - \Omega_{\Lambda}(a) + \left( 1 + \frac{\Omega_{\text{m}}(a)}{2} \right) \left( 1 + \frac{\Omega_{\Lambda}(a)}{70} \right) \right)^{-1}. \quad (10)$$

If  $m_{\nu} \neq 0$ , then we must correct this to describe the suppression by neutrinos. We will always assume that we have  $N_{\nu} = 3$

neutrinos when the neutrino mass is non-zero. One can then define the density parameters of neutrinos and cold dark matter as (Kolb & Turner 1990)

$$\Omega_{\nu} = \frac{m_{\nu}}{93.14 h^2}, \quad \Omega_{\text{c}} = \Omega_{\text{m}} - \Omega_{\text{b}} - \Omega_{\nu}, \quad (11)$$

and then the fractional parameters for each species as

$$f_{\text{c}} \equiv \frac{\Omega_{\text{c}}}{\Omega_{\text{m}}}, \quad f_{\text{b}} \equiv \frac{\Omega_{\text{b}}}{\Omega_{\text{m}}}, \quad f_{\nu} \equiv \frac{\Omega_{\nu}}{\Omega_{\text{m}}}, \quad f_{\text{cb}} \equiv f_{\text{c}} + f_{\text{b}}. \quad (12)$$

We then utilise the approximations for the effects of neutrinos on the growth factor of Bond et al. (1980); Hu & Eisenstein (1998), which are

$$p_{\text{cb}} = \frac{1}{4} \left( 5 - \sqrt{1 + 24 f_{\text{cb}}} \right), \quad (13)$$

$$\tilde{q} = \frac{kh\Theta_{2.7}^2}{\Omega_{\text{m}} h^2}, \quad (14)$$

$$y_{\text{fs}} = 17.2 f_{\nu} \left( 1 + \frac{0.488}{f_{\nu}^{7/6}} \right) \left( \frac{N_{\nu} \tilde{q}}{f_{\nu}} \right)^2, \quad (15)$$

$$D_{\text{cbv}}(k, a, \theta) = \left( f_{\text{cb}}^{0.7/p_{\text{cb}}} + \left( \frac{D_1(a, \theta)}{1 + y_{\text{fs}}} \right)^{0.7} \right)^{p_{\text{cb}}/0.7} D_1(a, \theta)^{1-p_{\text{cb}}}. \quad (16)$$

An approximation to the growth factor can then be written as

$$D_{\text{approx}}(k, a, \theta) = D_{\text{cbv}}(k, a, \theta) \left( 1 + z_{\text{eq}} \right)^{-1}, \quad (17)$$

where we choose a normalisation such that  $D_{\text{approx}} \rightarrow a$  as  $a \rightarrow 0$ .

### 5.2. $\Lambda$ CDM power spectrum

To give an approximate template for the matter power spectrum at redshift zero, we will use the results of Eisenstein & Hu (1998); Bartlett et al. (2024a). To do this, we define  $\omega_{\text{m}} \equiv \Omega_{\text{m}} h^2$  and  $\omega_{\text{b}} \equiv \Omega_{\text{b}} h^2$ , and define the following variables

$$s \equiv \frac{44.5 \log \left( \frac{9.83}{\omega_{\text{m}}} \right)}{\sqrt{1.0 + 10.0 \omega_{\text{b}}^{3/4}}}, \quad (18)$$

$$\alpha \equiv 1.0 - 0.328 \log(431.0 \omega_{\text{m}}) \omega_{\text{b}} + 0.38 \log(22.3 \omega_{\text{m}}) \omega_{\text{b}}^2, \quad (19)$$

$$\Gamma \equiv \Omega_{\text{m}} h \left( \alpha + \frac{1.0 - \alpha}{1.0 + (0.43 k h s)^4} \right), \quad (20)$$

$$\Theta_{2.7} = \frac{T_{\text{CMB}}}{2.7 \text{ K}}, \quad (21)$$

$$q \equiv k \Theta_{2.7} \Gamma^{-1} \quad (22)$$

$$C_0 \equiv 14.2 + \frac{731.0}{1 + 62.5 q} \quad (23)$$

$$L_0 \equiv \log(2e + 1.8 q), \quad (24)$$

where  $k$  is measured in  $h \text{ Mpc}^{-1}$  and  $T_{\text{CMB}}$  is the temperature of the CMB (which we assume to be 2.7255 K throughout (Mather et al. 1999)). Given this, one can write the Eisenstein & Hu ‘‘no-wiggles’’ power spectrum at  $z = 0$  as

$$P_{\text{EH}}(k, \theta_{\Lambda\text{CDM}}) = \frac{2\pi^2}{k^3} A_{\text{s}} \left( \frac{k}{k_{\text{pivot}}} \right)^{n_{\text{s}}-1} \left( \frac{2k^2 c^2}{5\Omega_{\text{m}}} \frac{L_0}{L_0 + C_0 q^2} \right)^2, \quad (25)$$

where  $k_{\text{pivot}} = 0.05 h \text{Mpc}^{-1}$ . This describes the overall envelope of the matter power spectrum correctly, but does not contain baryonic acoustic oscillations.

To approximate the redshift-zero power spectrum in  $\Lambda\text{CDM}$ , we define

$$P_{\Lambda\text{CDM}}(k, \theta_{\Lambda\text{CDM}}) \equiv P_{\text{EH}}(k, \theta_{\Lambda\text{CDM}})F(k, \theta_{\Lambda\text{CDM}}), \quad (26)$$

where we use the approximation of Bartlett et al. (2024a) to evaluate  $F(k, \theta)$ :

$$\begin{aligned} \log F = & b_0 h - b_1 + \left( \frac{b_2 \Omega_b}{\sqrt{h^2 + b_3}} \right)^{b_4 \Omega_m} \\ & \times \left[ \frac{b_5 k - \Omega_b}{\sqrt{b_6 + (\Omega_b - b_7 k)^2}} b_8 (b_9 k)^{-b_{10} k} \cos \left( b_{11} \Omega_m - \frac{b_{12} k}{\sqrt{b_{13} + \Omega_b^2}} \right) \right. \\ & \left. - b_{14} \left( \frac{b_{15} k}{\sqrt{1 + b_{16} k^2}} - \Omega_m \right) \cos \left( \frac{b_{17} h}{\sqrt{1 + b_{18} k^2}} \right) \right] \\ & + b_{19} (b_{20} \Omega_m + b_{21} h - \log(b_{22} k) + (b_{23} k)^{-b_{24} k}) \cos \left( \frac{b_{25}}{\sqrt{1 + b_{26} k^2}} \right) \\ & + (b_{27} k)^{-b_{28} k} \left( b_{29} k - \frac{b_{30} \log(b_{31} k)}{\sqrt{b_{32} + (\Omega_m - b_{33} h)^2}} \right) \\ & \times \cos \left( b_{34} \Omega_m - \frac{b_{35} k}{\sqrt{b_{36} + \Omega_b^2}} \right), \end{aligned} \quad (27)$$

where the parameters  $\mathbf{b}$  are given in Table 2 of Bartlett et al. (2024a). This approximation gives a linear power spectrum which has a root mean squared fractional error of 0.2% across the  $k$  values and  $\Lambda\text{CDM}$  portion of the parameter range considered in this work (Bartlett et al. 2024a) when multiplied by the appropriate linear growth factor.

### 5.3. SR corrections to the linear power spectrum

The approximations outlined in Sections 5.1 and 5.2 yield reasonable approximations to the matter power spectrum, but do not have sub-percent precision. Even when restricted to the  $\Lambda\text{CDM}$  subspace, since  $D_{\text{approx}}$  is only an approximation, we find that errors on  $P_{\text{lin}}(k)$  can still be up to a few percent. Therefore, in this section we use SR to correct for these errors.

#### 5.3.1. Corrections to the growth factor

To obtain a correction to the growth factor,  $R(a, \theta)$ , we generate two LHs of 2000 cosmologies from Table 1, one for training and one for validation. We used 200 logarithmically spaced  $k$  values in the range  $9 \times 10^{-3} - 9 h \text{Mpc}^{-1}$  and compute  $R$ , as defined in Eq. (6), and using the results of Sections 5.1 and 5.2. We find the mean over these  $k$  values, and this is then fitted as a function of cosmological parameters and scale factor using OPERON, where we search for expressions containing the operators  $+$ ,  $-$ ,  $\times$ ,  $\div$ ,  $\sqrt{\cdot}$  and  $\log$ . We allow a maximum model length of 100 and set  $\epsilon = 10^{-3}$ .

After running for 1 hour on 56 cores, we obtain the Pareto front plotted in Fig. 4. As with our  $\sigma_8$  emulator, we find very similar training and validation losses for all model lengths. The improvement in accuracy as one makes the model more complex

**Table 3.** Best-fit parameters for the correction to the growth factor approximation given in Eq. (28).

Param.	Value	Param.	Value	Param.	Value
$d_0$	0.8545	$d_6$	-0.4136	$d_{12}$	5.8014
$d_1$	0.394	$d_7$	1.4769	$d_{13}$	6.7085
$d_2$	0.7294	$d_8$	-0.5959	$d_{14}$	0.3445
$d_3$	0.5347	$d_9$	-0.4553	$d_{15}$	1.2498
$d_4$	-0.4662	$d_{10}$	-0.0799	$d_{16}$	0.3756
$d_5$	-4.6669	$d_{11}$	-5.8311	$d_{17}$	0.2136

slightly plateaus at a length of  $\sim 50$ , at which point the root mean squared error is below 0.1%. We therefore choose a model for  $R$  from this region of the Pareto front, and, after inspection, choose the model of length 53.

Although we defined  $R(a = 1, \theta) = 1 \forall \theta$ , the SR result does not return this exactly due to the finite precision of the parameters and the fact that this is only inferred from the training data, rather than strictly enforced during the search. As such, we find that some parameters which are approximately equal must be equated and that some parameters must be rounded in order to require this condition exactly. After performing such manipulations, we arrive at the following approximation for  $R(a, \theta)$

$$\begin{aligned} R(a, \theta) \approx & 1 + (1 - a) \left[ d_0 \right. \\ & \left. - \frac{1}{d_1 a + d_2 + (d_3 \Omega_m + d_4 a) \log(d_5 w_0 + d_6 w_a)} \right. \\ & \left. - \frac{d_7 \Omega_m + d_8 a + \log(d_9 w_0 + d_{10} w_a)}{d_{11} a + d_{12} + d_{13} (d_{14} \Omega_m + d_{15} a - 1) (d_{16} w_0 + d_{17} w_a + 1)} \right], \end{aligned} \quad (28)$$

where the parameters  $\mathbf{d}$  are given in Table 3. It is trivial to see that this equals unity at  $a = 1$  for any set of cosmological parameters.

This expression is interesting since, although we allowed OPERON to obtain a function of any combination of cosmological parameters, we find that only  $\Omega_m$ ,  $w_0$  and  $w_a$  appear in Eq. (28). Given that these are the parameters which govern the expansion history (alongside  $h$ ), this suggests that this equation is correcting for the mistakes made in modelling the background expansion when using  $D_{\text{approx}}$ . Although  $m_\nu$  do not appear in this equation, it does not mean that there is no time-dependence in the effects of neutrino suppression on  $P_{\text{lin}}(k, a, \theta)$ , but just that  $D_{\text{approx}}$  captures this effect sufficiently well for sub-percent level predictions.

#### 5.3.2. Corrections to the present-day linear power spectrum

The next step is to obtain a correction,  $S(k, \theta)$ , to the redshift-zero power spectrum. This correction depends on  $k$ , therefore the training set size is expanded by the number of  $k$  values, making it challenging to use a large training size. We found that LHs of 200 cosmologies with 200 logarithmically spaced  $k$  values in the range  $9 \times 10^{-3} - 9 h \text{Mpc}^{-1}$  is sufficient for training an accurate  $S(k, \theta)$ . We then compute  $S$ , as defined in Eq. (6), and using the results of Sections 5.1 and 5.2. We choose our target variable to be  $10 \log_{10} S(k, \theta)$  so that (i) the emulated  $S(k, \theta)$  will always be positive, (ii) a root mean squared error on the target corresponds to minimising the fractional error on  $S(k, \theta)$ , and (iii) we introduce the factor of 10 to make the target closer to unity. This is then fitted as a function of cosmological parameters and  $k$  values using OPERON, where we search for expressions containing the operators  $+$ ,  $-$ ,  $\times$ ,  $\div$ ,  $\sqrt{\cdot}$ ,  $\log$ ,  $\cos$ ,  $\text{pow}$  and analytic quotient

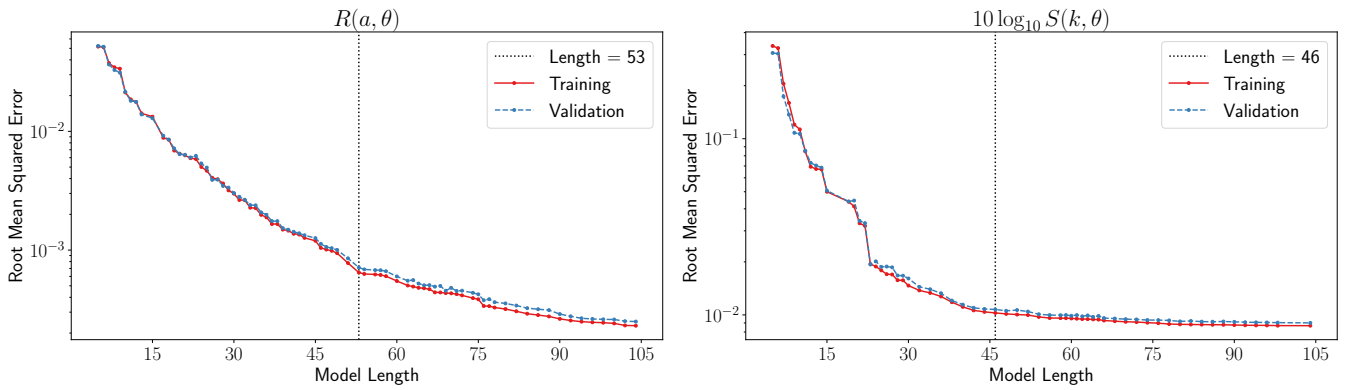


**Fig. 4.** Pareto front of solutions for the correction to the growth factor,  $R(a, \theta)$ , (left), and the correction to the redshift-zero matter power spectrum,  $10 \log_{10} S(k, \theta)$ , (right) as found by OPERON. The chosen models are indicated by the vertical lines, and we plot the root mean squared errors on the predictions for the training and validation sets separately.

operators ( $\text{aq}(x, y) \equiv x / \sqrt{1 + y^2}$ ). We allow a maximum model length of 100 and set  $\epsilon = 10^{-3}$ .

After running for 6 hour on 56 cores, we obtain the Pareto front plotted in Fig. 4. We see that the Pareto front is considerably flatter for large model lengths than the previous cases, namely that there is little improvement in accuracy when one makes the model more complex. We therefore choose an expression from the start of the flat region of the Pareto front, and find that the expression at length 46 is appropriate for our purposes.

As well as merging and removing superfluous parameters, we find that it is necessary to remove one term from this equation. The expression found by OPERON contained a term which, when we evaluate the model for a  $\Lambda$ CDM universe, was proportional to  $k$ . Given that the expression from Bartlett et al. (2024a) is a good approximation for  $\Lambda$ CDM universes, one would expect that  $S(k, \theta)$  would be independent of  $k$  for these cosmologies, and would simply scale the growth factor to correct for the mistakes obtained when using an approximate version, since the shape of  $P_{\text{lin}}(k, a, \theta)$  should be correct. Since the coefficient for this  $k$ -dependent term was small ( $O(10^{-4})$ ), we set this coefficient to zero to remove this term. After removing this term, we re-optimised the coefficients of the function using the training set. We find that the omission of this term has a negligible effect on the accuracy of the expression.

After performing these manipulations, we arrive at the expression

$$10 \log_{10} S(k, \theta) \approx -e_0 h - e_1 w_0 - \frac{e_2 m_\nu}{\sqrt{e_3 + k^2}} - \frac{e_4 h}{e_5 h + m_\nu} + \frac{e_6 m_\nu}{h \sqrt{e_7 + (e_8 \Omega_m + k)^2}} + \frac{e_9 \Omega_b - e_{10} w_0 - e_{11} w_a + \frac{e_{12} w_0 + e_{13}}{e_{14} w_a + w_0}}{\sqrt{e_{15} + (\Omega_m + e_{16} \log(-e_{17} w_0))^2}}. \quad (29)$$

when the coefficients  $e$  are tabulated in Table 4.

There are several interesting features in this approximation. Firstly, let us consider the  $\Lambda$ CDM limit, where we have  $w_0 = -1$ ,  $w_a = 0$  and  $m_\nu = 0$

$$10 \log_{10} S_{\Lambda\text{CDM}} = -e_0 h + e_1 - \frac{e_4}{e_5} + \frac{e_9 \Omega_b + e_{10} + e_{12} - e_{13}}{\sqrt{e_{15} + (\Omega_m + e_{16} \log e_{17})^2}}, \quad (30)$$

which is not zero, and thus we have a correction even for these cosmologies. Given that  $R(a, \theta)$  is unity at redshift zero so can-

not correct for errors in  $D_{\text{approx}}$ , this term gives a correction to the growth factor at  $a = 1$  due to using an approximation to this. This term provides a correction to the result of Bartlett et al. (2024a), as given in Eq. (27). This  $k$ -independent correction adjusts the normalisation of the redshift-zero linear power spectrum, which arises since Bartlett et al. (2024a) fitted the residuals between CAMB and the Eisenstein & Hu prediction, as returned by the COLOSSUS package. In COLOSSUS, the normalisation is set such that the result of computing Eq. (2) with the approximate power spectrum matches the desired  $\sigma_8$ . Given the limitations of the Eisenstein & Hu approximation, this induces a multiplicative scaling to the power spectrum which can given errors of a few percent on large scales (i.e. if one inferred  $A_s$  from the low- $k$  behaviour of the COLOSSUS power spectrum, one would find a value which is wrong by a few percent). Although Eq. (27) removes this offset, since in this work we do not attempt to match  $\sigma_8$  in this way, Eq. (30) acts to reintroduce this offset so that Eq. (27) yields the correct result.

Let us also consider the limiting behaviour of Eq. (29). On large scales ( $k \rightarrow 0$ ), one observes that  $S(k, \theta)$  tends to a constant, and thus introduces a multiplicative correction due to imperfections induced by the other approximations. It is essential that there is no  $k$ -dependence in this limit, since the power spectrum must be proportional to  $k^{n_s}$  on large scales, and this is already captured by Eq. (25). We also note that on small scales ( $k \rightarrow \infty$ ),  $S(k, \theta)$  also tends to a (different) constant. This implies that the other terms in the approximation yield the correct  $k$ -dependence on small scales. We note that it is desirable that this term does not diverge even when extrapolated to large  $k$ , which is neither guaranteed nor analytically testable for a numerical emulator.

Finally, we note that, although we allowed such behaviour, Eq. (29) does not contain any oscillatory terms. This is understandable since one would not expect the interaction between photons and baryons which give rise to the BAO features to depend on the nature of dark energy nor the sum of neutrino masses: these additional components should only affect the broad-band features of the power spectrum. This is indeed what we find, and further justifies our decision to find a correction to the  $\Lambda$ CDM result from Bartlett et al. (2024a) rather than refit the whole equation, given the (hard to fit) oscillatory features are unchanged.



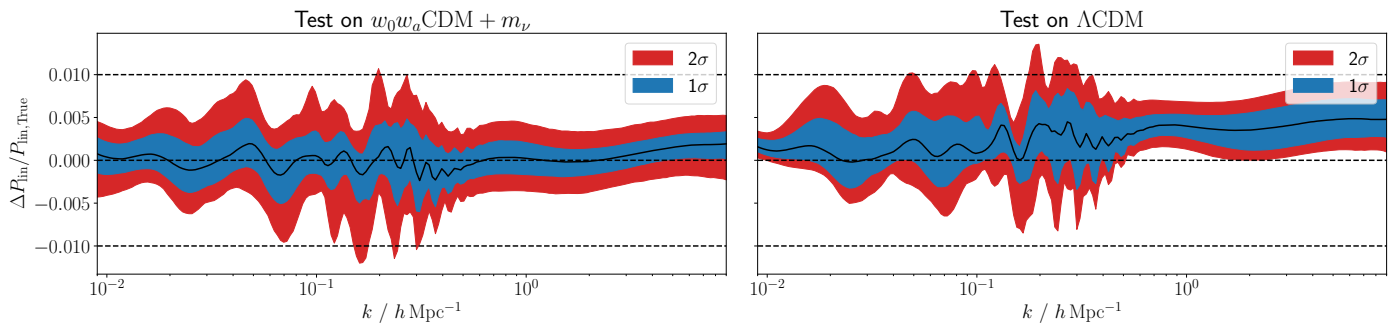


**Fig. 5.** Distribution of fractional errors on  $P_{\text{lin}}(k, a, \theta)$  as a function of  $k$  for the extended cosmological models considered in this work (left) and for  $\Lambda\text{CDM}$  (right). The bands given the 1 and  $2\sigma$  values across the LH (Table 1), with the dashed lines indicating 1% error. When averaged over  $k$ , we find that our expressions have a root mean squared error of 0.28% for the extended cosmology, and 0.41% for  $\Lambda\text{CDM}$ .

**Table 4.** Best-fit parameters for the correction to the linear power spectrum given in Eq. (29).

Param.	Value	Param.	Value	Param.	Value
$e_0$	0.2841	$e_6$	0.0985	$e_{12}$	0.1385
$e_1$	0.1679	$e_7$	0.0009	$e_{13}$	0.2825
$e_2$	0.0534	$e_8$	0.1258	$e_{14}$	0.8098
$e_3$	0.0024	$e_9$	0.2476	$e_{15}$	0.019
$e_4$	0.1183	$e_{10}$	0.1841	$e_{16}$	0.1376
$e_5$	0.3971	$e_{11}$	0.0316	$e_{17}$	0.3733

### 5.3.3. Performance of combined approximation

Now that we have verified that the individual components of the linear matter power spectrum are accurately approximated, we combine these approximations to assess the performance of  $P_{\text{lin}}(k, a, \theta)$  across the cosmologies and redshifts considered in this work. Using a LH of 2000 points from the prior range in Table 1, we compare the predictions from the expressions obtained in this work to the true linear power spectrum, as computed using CLASS. We consider both the full parameter space and a separate LH where we restrict ourselves to  $\Lambda\text{CDM}$  only. The resulting distribution of errors as a function of  $k$  are plotted in Fig. 5, where the bands correspond to the 68<sup>th</sup> and 95<sup>th</sup> percentiles of errors across the test set at a given  $k$ . Again, we consider 200 values of  $k$  which are logarithmically spaced between  $9 \times 10^{-3}$  and  $9 h \text{Mpc}^{-1}$ .

We find that the root mean squared error at any given value of  $k$  is much less than 1%, and is 0.28% for the full parameter space when averaged over  $k$  and redshift. This increases to 0.41% when we consider the  $\Lambda\text{CDM}$  sub-space, which is approximately a factor of 2 less accurate than the approximation of Bartlett et al. (2024a). We attribute this the fact that zero neutrino mass is towards the edge of the range of our training set, where one would expect less accurate results. We explore this point further in Section 7.2. Nonetheless, we find that the  $2\sigma$  error band when varied as a function of  $k$  is almost always within 1%. We assess the performance of this approximation further in Section 7.1, where we compare to other emulators and fitting functions.

## 6. Analytic emulator for the nonlinear power spectrum

Now that we have symbolic emulators for quantities related to the linear power spectrum, in this section we aim to produce an

approximation for the nonlinear case. To obtain such an expres-

sion, one must have access to  $P_{\text{nl}}(k, a, \theta)$  for a range of cosmological parameters and redshifts. As in Bartlett et al. (2024b), we obtained these by evaluating EUCLIDEMULATOR2 (Euclid Collaboration et al. 2021), a method known for its speed and accuracy in predicting the ratio of the nonlinear to linear matter power spectrum. This approach was preferred over generating new  $N$ -body simulations, as it is significantly less computationally demanding. EUCLIDEMULATOR2 provides percent-level accuracy, allowing us to fit the emulated spectra with high precision and offering greater flexibility in selecting redshift values. Our results are validated against  $N$ -body simulations, as discussed in Section 7.1.

Unlike Bartlett et al. (2024b), where corrections are applied to an existing HALOFIT formalism, our approach directly fits the nonlinear power spectrum,  $P_{\text{nl}}$ , as a function of  $k$ ,  $a$ ,  $\theta$ , and  $P_{\text{lin}}(k, a, \theta)$ . By doing this, we avoid fitting additional HALOFIT variables, which can introduce further uncertainties. This method provides a more straightforward and potentially more accurate model for predicting the nonlinear power spectrum, since we do not have to correct for mistakes made by using a previous approximation.

Similar to  $S(k, \theta)$ , we used a Latin hypercube sampling of 200 cosmologies with 200 logarithmically spaced  $k$  values in the range  $9 \times 10^{-3} - 9 h \text{Mpc}^{-1}$  to generate the training set. For each cosmology, we generated the corresponding nonlinear power spectrum using EUCLIDEMULATOR2. Since the nonlinear emulator requires  $P_{\text{lin}}$  as input, during training we used ground truth values computed by CLASS. However, for evaluating performance, we employed the  $P_{\text{lin}}$  emulator developed in Section 5.

We fit the nonlinear power spectrum  $P_{\text{nl}}(k, a, \theta, P_{\text{lin}})$  using OPERON. The model searches for expressions composed of the operators  $+$ ,  $-$ ,  $\times$ ,  $\div$ ,  $\sqrt{\cdot}$ ,  $\log$ , and  $\text{pow}$ . We found that excluding the analytic quotient operator improves the limiting behaviour, as it is easier to enforce the correct limits (discussed below) to the found expressions when this operator was removed. We set our target to  $\log_{10} P_{\text{nl}}$  and transform the input  $P_{\text{lin}}$  to  $\log_{10} P_{\text{lin}}$  as well. We allow a maximum model length of 200, and we use the root mean squared error as the loss function, with  $\epsilon = 10^{-3}$ . After running for 24 hours on 56 cores, we obtain the Pareto front shown in Fig. 6. From this, we select the expression with a model length of 73. The resulting equation is:

$$\log_{10} \tilde{P}_{\text{nl}} = \log_{10} P_{\text{lin}} + \frac{g_0 k (g_1 k)^{g_2 \Omega_m - g_3 \times 10^9 A_s}}{(g_4 k^{-g_5} - g_6 \log_{10} P_{\text{lin}})^{g_7 \log_{10} P_{\text{lin}} + g_8 w_a + g_9 w_0 - g_{10}} + (g_{11} k^{g_{12}} + g_{13} \log_{10} P_{\text{lin}} - g_{14} \Omega_m)^{g_{15} a - g_{16} n_s}} + \frac{(g_{17} a - g_{18} \log_{10} P_{\text{lin}} + g_{19}) k}{g_{20} \Omega_m + g_{21} k + g_{22} n_s - g_{23} + (g_{24} \log_{10} P_{\text{lin}} + g_{25} k^{g_{26}})^{g_{27} a - g_{28} n_s}} - g_{29} k - (g_{30} k)^{(g_{31} k)^{-g_{32}}}, \quad (31)$$

where the best-fit parameters are given in Table 5. We denote this expression  $\tilde{P}_{\text{nl}}$  rather than  $P_{\text{nl}}$ , since it is not our final approximation for the nonlinear power spectrum (see Eq. (33) below).

We find that this equation has several interesting properties. Firstly, one can analytically check the limiting behaviour as  $k \rightarrow 0$ . In this case, we find that  $P_{\text{nl}} \rightarrow P_{\text{lin}}$  as  $k \rightarrow 0$ , consistent with our theoretical interpretation. It would not be possible to guarantee such behaviour using purely numerical emulators. Second, we observe that  $m_\nu$  does not appear explicitly; its dependence is only implicit through  $P_{\text{lin}}$ . This aligns with the results of Bayer et al. (2022), who found that all the information on the neutrino mass in the large scale structure is encoded in the linear power spectrum, and not the nonlinear evolution.

When evaluated on both the training and validation set, we observed that this equation by itself introduces a systematic offset compared to the EUCLIDEMULATOR2 results across all cosmologies and redshifts. This is a result of a sub-optimal search of the genetic algorithm, since it was unable to correct for this residual. Therefore, we introduced a post-processing step to correct for this, where we fitted and subtracted the offset from the prediction. Again using OPERON with the same settings as before, we fit for the offset as a function of  $k$  only. We find that the equation

$$\text{offset}(k) = \frac{h_0 + (h_1 k - \cos(h_3 \cos(h_2 k))) \cdot \cos(h_4 k) + \cos(h_5 k)}{-h_7 \cdot \log(h_6 k) + h_8 k}, \quad (32)$$

where  $\mathbf{h} = [0.5787, 2.3485, 27.3829, 16.4236, 97.3766, 90.9764, 11.2046, 2447.2, 11376.93]$ , is sufficient to capture the remaining residual. The final equation for nonlinear power spectrum is then given by

$$\log_{10} P_{\text{nl}} = \log_{10} \tilde{P}_{\text{nl}} - \text{offset}(k). \quad (33)$$

Note that this offset does not affect the limiting behaviour as  $k \rightarrow 0$ , since the offset tends to zero as  $k \rightarrow 0$ . For large  $k$ , we find that this offset term does not exactly tend to zero, but oscillates around  $h_1/h_8 \approx 2 \times 10^{-4}$  with a period  $\Delta k = 2\pi/h_4 \approx$

**Table 5.** Best-fit parameters for nonlinear power spectrum given in Eq. (31).

Param.	Value	Param.	Value	Param.	Value
$g_0$	0.2107	$g_{11}$	0.9039	$g_{22}$	1.4326
$g_1$	0.0035	$g_{12}$	0.0749	$g_{23}$	1.8971
$g_2$	0.0667	$g_{13}$	0.0741	$g_{24}$	0.0271
$g_3$	0.0442	$g_{14}$	0.1277	$g_{25}$	0.9635
$g_4$	1.2809	$g_{15}$	27.6818	$g_{26}$	0.0264
$g_5$	0.2287	$g_{16}$	24.8736	$g_{27}$	22.9213
$g_6$	0.1122	$g_{17}$	0.6264	$g_{28}$	71.1658
$g_7$	4.3318	$g_{18}$	0.3035	$g_{29}$	0.0371
$g_8$	1.1857	$g_{19}$	0.6069	$g_{30}$	0.0099
$g_9$	3.3117	$g_{20}$	0.7882	$g_{31}$	210.3925
$g_{10}$	14.2829	$g_{21}$	0.4811	$g_{32}$	0.2555

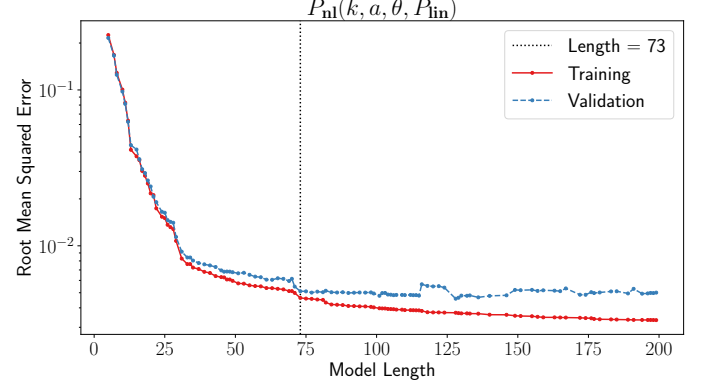


**Fig. 6.** Same as Fig. 4 but for  $\log_{10} P_{\text{nl}}(k, a, \theta, P_{\text{lin}})$ .

$0.06 h \text{ Mpc}^{-1}$ . Such oscillations give a maximum correction to  $\tilde{P}_{\text{nl}}$  of 0.05%, which is much smaller than the error on the power spectrum, and the variation with  $k$  is much finer than the values of  $k$  for which we reach this limit, which effectively averages out these oscillations. As such, we find that this offset becomes negligible as  $k \rightarrow \infty$ .

Using a LH of 2000 points from the prior range in Table 1, we compare our expressions' predictions to the outputs from EUCLIDEMULATOR2, considering both the full parameter space and a restricted  $\Lambda$ CDM model. The results are given in Fig. 7. The root mean squared fractional error for the two cases is 1.3% and 1.1%, respectively. We find that, in both cases, the error is dominated by the prediction at large  $k$ , where the  $1\sigma$  difference between our result and EUCLIDEMULATOR2 can exceed 1%, whereas the two emulators agree within 1% before  $k \sim 1 h \text{ Mpc}^{-1}$ . Due to the inclusion of Eq. (32), when compared to Figure 5 of Bartlett et al. (2024b), we find that the residuals of our emulator at the BAOs are smaller and that the mean difference is much closer to zero.

To assess whether this level of disagreement is acceptable, we compare the difference between our symbolic emulator and EUCLIDEMULATOR2 to that between the numerical emulators BACCO and EUCLIDEMULATOR2 over the LH used in this work. In Fig. 8 we plot the  $1\sigma$  errors across the hypercube for both methods, where we see both our result and BACCO agree within 1% as we go to  $k \rightarrow 0$ , as should be expected given that both methods produce sub-percent accurate linear power spectra. Around the scale of the BAOs, the level of disagreement with EUCLIDEMULATOR2 slightly increases to approximately 1% for both emulators. As we increase  $k$  further to  $k > 1 h \text{ Mpc}^{-1}$ , we find that our error is relatively stable at around 1%, whereas the discrepancy between EUCLIDEMULATOR2 and BACCO rises dramatically to around 4% by  $k \sim 4 h \text{ Mpc}^{-1}$ . As such, we conclude that the level of disagreement between our approximation and EUCLIDEMULATOR2 is comparable to that between current numerical emulators, and thus we have reached a sufficiently accurate solution. We investigate what this level of disagreement corresponds to for weak lensing measurements in Section 7.3.

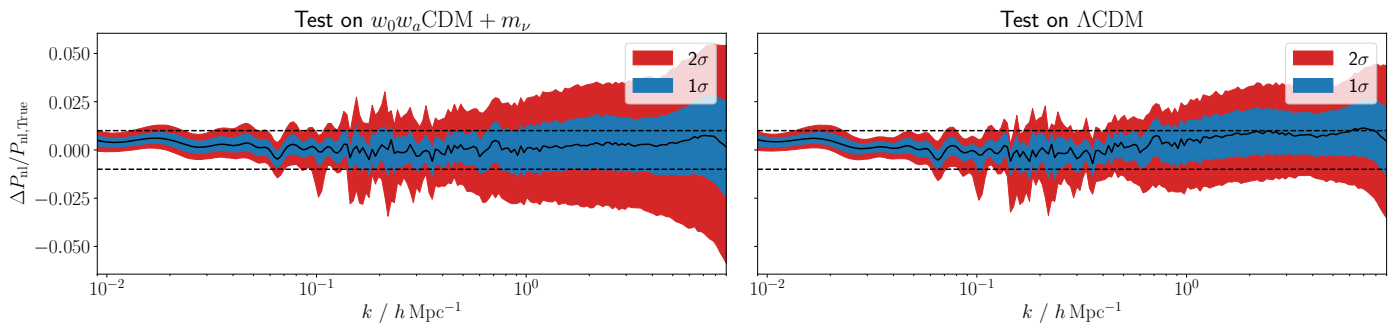


**Fig. 7.** Same as Fig. 5 but for  $P_{\text{nl}}(k, a, \theta, P_{\text{lin}})$ , where we plot the errors relative to EUCLIDEMULATOR2. When averaged over  $k$ , we find that our expressions have a root mean squared error of 1.3% for the extended cosmology, and 1.1% for  $\Lambda$ CDM.

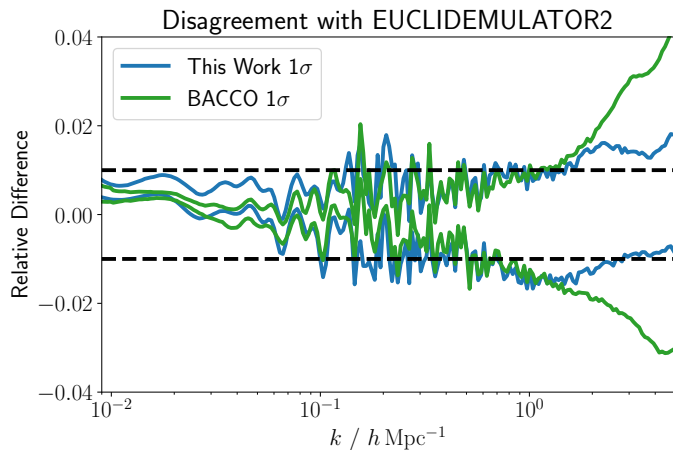


**Fig. 8.** Distribution of fractional differences between different emulators. As a reference we use EUCLIDEMULATOR2, and show the differences between this and the symbolic approximation obtained in this work and the BACCO emulator. We plot the  $1\sigma$  differences across the LH used in this work, and the dashed lines correspond to 1% agreement. The difference between our result and EUCLIDEMULATOR2 is comparable to the differences between the numerical emulators.

## 7. Performance of emulators

### 7.1. Comparison against other emulators

In this section we assess the performance of our emulator against those from the literature in terms of both run time and accuracy. To assess accuracy, for  $P_{\text{lin}}(k, a, \theta)$ , we compare the predicted power spectra to that computed by CLASS. For the nonlinear case, however, it is less obvious what the standard against which we should compare is. In Section 6, we calibrated our emulator against EUCLIDEMULATOR2 since this provided a computationally cheap way of generating a large number of spectra at a range of redshifts. Now, however, we wish to compare against a  $N$ -body simulation, otherwise, by construction, EUCLIDEMULATOR2 would have zero error. Therefore, as in Bartlett et al. (2024b), we benchmark the nonlinear emulators against the QUIJOTE suite of simulations (Villaescusa-Navarro et al. 2020).

In particular, we test the accuracy against the following four sets simulations

1. *Fiducial*: This simulation has a  $\Lambda$ CDM cosmology with the *Planck* 2018 cosmological parameters (Planck Collaboration 2020):  $\Omega_{\text{m}} = 0.3175$ ,  $\Omega_{\text{b}} = 0.049$ ,  $h = 0.6711$ ,  $n_{\text{s}} = 0.9624$ ,  $\sigma_8 = 0.834$ ,  $m_{\nu} = 0$ ,  $w_0 = -1$ ,  $w_a = 0$ .
2.  $M_{\nu}^+$ : This simulation has a cosmological constant for dark energy, but contains three degenerate massive neutrino

species of total mass  $m_{\nu} = 0.1$  eV. All other parameters are the same as for the *Fiducial* simulation.

3.  $w^+$ : In this simulation the dark energy equation of state is constant in time, but equal to  $-1.05$  ( $w_0 = -1.05$ ,  $w_a = 0$ ). All other parameters are the same as for the *Fiducial* simulation.
4.  $w^-$ : This is the same as the  $w^+$  simulation, except  $w_0 = -0.95$ .

All simulations contain  $N^3 = 512^3$  particles within a cubic box of side length  $L = 1 h^{-1}$  Gpc, and were run using the GADGET-III code (Springel 2005). The simulations containing neutrinos contain an additional  $512^3$  neutrino particles. We make use of the publicly available power spectra for these simulations for  $k \in [0.02, 0.5] h \text{ Mpc}^{-1}$ , since we expect these to be converged in this range (Bartlett et al. 2024b). To remove the effects of cosmic variance (i.e. to obtain an estimate of the ensemble mean power spectra), we average these spectra across all available simulations in each suite (15,000 for the *Fiducial* simulation and 5,000 for the others).

We first compare various linear power spectrum emulators across the four cosmologies. The emulators considered are BACCO (Angulo et al. 2021; Aricò et al. 2021; Zennaro et al. 2023), COSMOPOWER (Spurio Mancini et al. 2022), and three equation-based models from previous works: Eisenstein & Hu (1998), Bartlett et al. (2024a), and Bayron Orjuela-Quintana et al. (2024). Each emulator is applied only to cosmologies that fall within its defined parameter space. Since COSMOPOWER can only be evaluated at fixed  $k$  values, we apply linear interpolation to enable comparisons on arbitrary  $k$ . Fig. 9 shows the relative error as a function of wavenumber  $k$  across different cosmologies at redshift 0.

Among the emulators considered, only BACCO and this work can be applied to all four cosmologies, and they show similar errors across the board, which is much less than 1% for all  $k$ . For the fiducial cosmology, the numerical emulators (BACCO and COSMOPOWER), the symbolic approximation of Bartlett et al. (2024a), and this work have power spectra which remain within 1% for all  $k$ , suggesting these all have the requisite accuracy for modern cosmological analyses. This is not the case for the Eisenstein & Hu (1998) and Bayron Orjuela-Quintana et al. (2024) formulae, whose errors can reach several percent, and are particularly large near the BAOs. Although they have the correct limiting behaviour by construction as  $k \rightarrow 0$ , their errors are much larger than what is required for current and future surveys (Taylor et al. 2018).

To assess the relative runtime of the emulators, we evaluated the linear power spectrum at redshift 1 for the four cosmologies mentioned above, performing  $10^3$  evaluations on an Intel Xeon E5-4650 CPU. We report the mean execution time per evaluation. The calculation used 200 logarithmically spaced values of

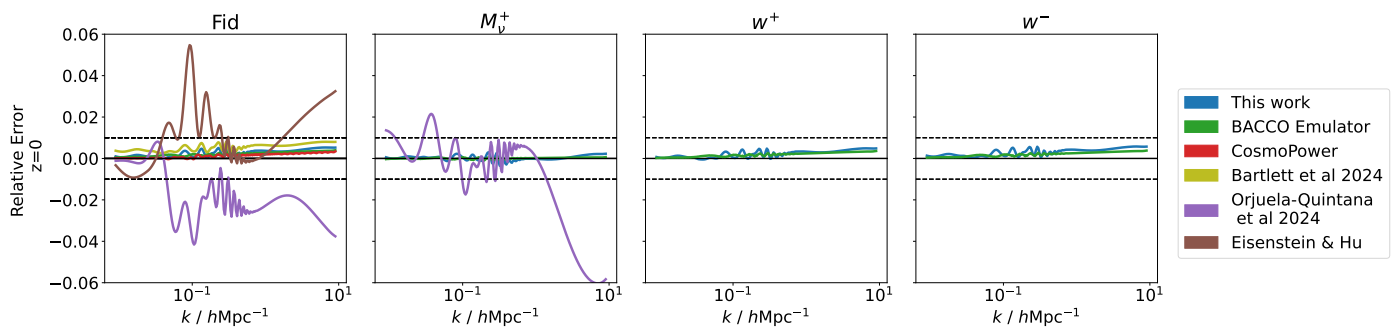


**Fig. 9.** Fractional error on the linear power spectrum as a function of wavenumber,  $k$ , for various emulators at redshift 0. We apply each emulator only to test data that falls within its defined parameter space.

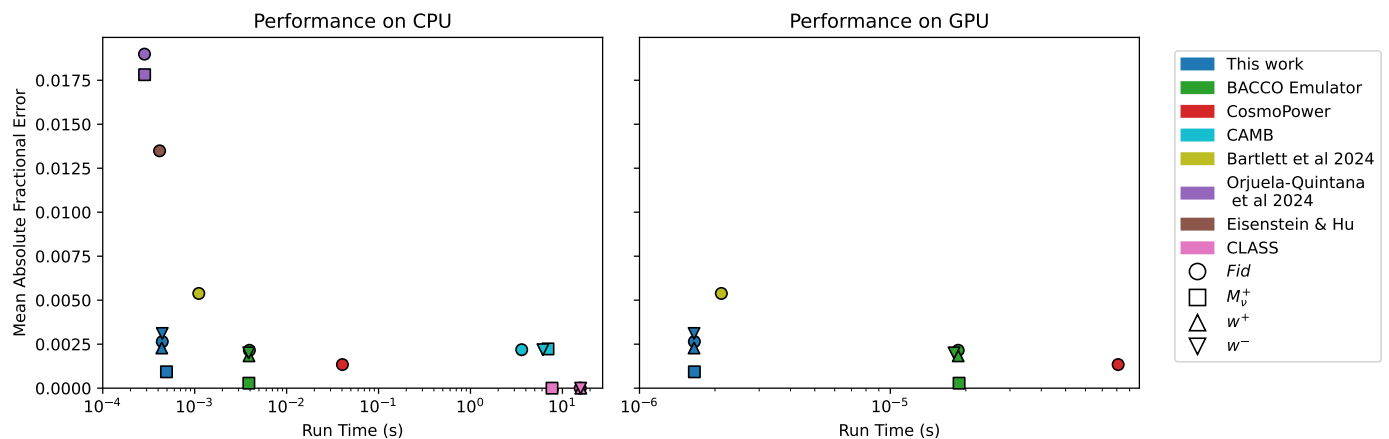


**Fig. 10.** Mean absolute fractional error (averaged over 200 logarithmically spaced  $k \in [9 \times 10^{-3}, 9] h \text{ Mpc}^{-1}$ ) with respect to CLASS against run time for various linear power spectrum emulators at four cosmologies and redshift 0. Some emulators are tested on both CPU (left panel) and GPU (right panel). The different colours refer to the emulator used, whereas each cosmology (defined in Section 7.1) is denoted by a different symbol.

$k$  in the range  $k = 9 \times 10^{-3} - 9 h \text{ Mpc}^{-1}$ . We assumed the availability of either  $A_s$  or  $\sigma_8$ , depending on the emulator’s requirements.

The results of this timing test are shown in Fig. 10, where we plot accuracy – computed as the mean absolute fractional error (averaged over  $k$ ) at redshift 1 across the four cosmologies – against runtime. Our emulator exhibits similar errors (within approximately 0.3%) to BACCO and COSMOPOWER, while being 8 and 80 times faster than them, respectively, on the CPU. Additionally, we include the runtime of two simulators, CLASS and CAMB, showing their differences in simulating the linear power spectrum. We find that our emulator obtains similar errors as there are discrepancies between the two codes (note that by definition CLASS has zero error in Fig. 10), but is a factor  $3 \times 10^4$  faster. Although they are of comparable speed to SYREN-HALOFIT and this work, the alternative analytic approximations of Eisenstein & Hu (1998, 1999); Bayron Orjuela-Quintana et al. (2024) are significantly less accurate, with mean errors much greater than a percent, and maximum errors of several percent (see Fig. 9). We find that the result of this work is faster than Bartlett et al. (2024a), which is to be expected given that we have removed the integral associated with using the COLOSSUS package (see Section 5.3.2).

Two of the emulators (BACCO and COSMOPOWER) are implemented in TensorFlow, making them more efficient for GPU execution. To account for this, we compare a PyTorch implementation of our emulator and of SYREN-HALOFIT with BACCO and COSMOPOWER. We run these four emulators on an NVIDIA Tesla V100 GPU, using a batch size of 2000 for each emulator, and compare their performance. The results are shown in the right panel of Fig. 10, where we see that all emulators are signifi-

cantly faster. However, due to its simplicity, we still find that our emulator is an order of magnitude faster than both COSMOPOWER and BACCO, with an evaluation time of less than  $2 \mu\text{s}$ . Again, we find SYREN-NEW to be faster than SYREN-HALOFIT.

We also conducted similar comparisons with several non-linear emulators: EUCLIDEMULATOR2 (Euclid Collaboration et al. 2021), BACCO (Angulo et al. 2021; Aricò et al. 2021; Zennaro et al. 2023), COSMOPOWER (Spurio Mancini et al. 2022), SYREN-HALOFIT (Bartlett et al. 2024b), and the HALOFIT (Smith et al. 2003; Bird et al. 2012; Takahashi et al. 2012) implementation in CLASS. EUCLIDEMULATOR2 and BACCO are trained to predict the ratio of the power spectrum of  $N$ -body simulations to the linear one, whereas COSMOPOWER replicates the results of HMCODE (Mead et al. 2021), which is a semi-analytic approach based on the halo model. These emulators were compared against QUIJOTE simulations across four suites and at three different redshifts (0, 0.5 and 1.5). Since COSMOPOWER has two additional free parameters –  $c_{\text{min}}$ , which describes the minimum halo concentration, and  $\eta_0$ , which determines the halo bloating – we optimise these parameters to minimise the mean squared error between the prediction of  $\log_{10} P_{\text{nl}}$  and that from QUIJOTE. The timing results for COSMOPOWER do not include this optimisation time and refers to a single pass once  $c_{\text{min}}$  and  $\eta_0$  are known.

The results, shown in Fig. 11 as absolute fractional errors, indicate that our emulator performs similarly to EUCLIDEMULATOR2 and BACCO across all suites. SYREN-HALOFIT is applicable only to the fiducial case and shows comparable errors to our method. In contrast, COSMOPOWER and CLASS-HALOFIT generally exhibit larger errors compared to our results. Fig. 12 displays the timing re-

sults against the mean absolute fractional error. Our emulator is shown to be 40 times faster than `BACCO` and  $10^4$  times faster than `EUCLIDEMULATOR2` on a CPU, all while maintaining comparable error levels. As before, we also compare a PyTorch implementation of our emulator with the two TensorFlow-based emulators in the right panel. We find that our emulator is 65 times faster than `COSMOPOWER` and 33 times faster than `BACCO`, and again takes approximately  $2 \mu\text{s}$  to evaluate.

## 7.2. Error distribution

Our results demonstrate that our linear emulator can achieve a root mean squared fractional error of less than 0.3%, and this is around 1% for the nonlinear emulator on the test set, which is sampled from our wide prior range. However, in applications such as inference problems, accuracy around the true cosmology is often more critical. To illustrate how the error varies with the distance from our current best-fit cosmology, we use cosmological constraints from the *Planck* + BAO + RSD + SN + DES chains of Alam et al. (2021). Specifically, we fit the marginal posteriors using a multivariate Gaussian distribution and define the distance of a given model from the fiducial one as the probability density provided by the Gaussian. For interpretability, we express this distance in terms of  $\sigma$  values. We generate several new test sets within 1, 3, 5, 7, and  $9\sigma$ , sampling parameters to be uniformly distributed in this range. Additionally, we compare these results to errors across the entire prior space.

The Alam et al. (2021) study does not provide posteriors that include all three of the  $w_0$ ,  $w_a$  and  $m_\nu$  parameters. Consequently, we cannot directly define a distance metric in our parameter space using their results. Therefore, we consider two subspaces of the 8-dimensional prior space: the  $\Lambda$ CDM parameters ( $A_s, \Omega_m, \Omega_b, h, n_s$ ) combined with  $w_0$  and  $w_a$ , and the  $\Lambda$ CDM parameters combined with  $m_\nu$  and  $w_0$ . These two posteriors define the distance in their respective subspaces, while we fix the remaining parameters as assumed by Alam et al. (2021).

Fig. 13 displays the distribution of errors as a function of distance from the best-fit model. For the  $w_0w_a$ CDM model, we find that the error decreases as we approach the centre of the posterior, such that the error on the linear power spectrum is below 0.2% within  $1\sigma$  of the posterior mean, and this is below 0.5% for the nonlinear case, which is over a factor of two better than across the full prior range.

In the  $w_0$ CDM+ $m_\nu$  subspace, although the error is smaller near the centre compared to the uniformly sampled test set, it increases slightly when approaching the  $m_\nu = 0$  point. This increase is due to the boundary effect in training: the lower limit for  $m_\nu$  in the training set is  $m_\nu = 0$ , which is problematic since we find empirically that our predictions typically become less accurate near the training set boundaries. For example, we see in Fig. 5 that the massless neutrino model has slight bias when we assume a cosmological constant for dark energy. Nonetheless, in the  $w_0$ CDM+ $m_\nu$  subspace, the error within  $9\sigma$  of the posterior mean is below 0.3% for the linear power spectrum and still a factor of 2 smaller than for the full prior range when considering the nonlinear emulator.

## 7.3. Performance for weak lensing analysis

In Section 6 and Section 7.1, we found that the discrepancy between other emulators or  $N$ -body simulations and our approximations is approximately at the percent-level for the nonlinear matter power spectrum, and that this difference is greatest at

large  $k$ . In this section, we wish to see what this 1% disagreement translates into when we move from just  $P(k)$  to precisely analysing cosmological observations from an upcoming large scale structure survey and to determine whether this is acceptable or not.

We focus on the upcoming weak lensing observations from the Rubin observatory’s Legacy Survey of Space and Time (LSST) (LSST Science Collaboration et al. 2009), which directly probes the matter power spectrum. We assess the performance of the model for two stages of the planned observations, year 1 (denoted as LSST Y1) and year 6 (denoted as LSST Y6). Following The LSST Dark Energy Science Collaboration et al. (2018), we assume that LSST Y1 will cover a sky area of  $f_{\text{sky}} = 0.3$  and that this will increase to  $f_{\text{sky}} = 0.4$  for Y6 analyses.

For these observations, the source samples are expected to follow a distribution given by

$$n_k^{\text{tot}}(z) \propto z^2 \exp[-(z/z_{\text{pz};0})^{\alpha_{\text{pz}}}], \quad (34)$$

which is normalised by the effective number density  $\bar{n}_k^{\text{tot}}$ . For LSST Y1, we assume  $\bar{n}_k^{\text{tot}} = 11.2$ ,  $\alpha_{\text{pz}} = 0.87$ , and  $z_{\text{pz};0} = 0.191$ ; for LSST Y6, we assume  $\bar{n}_k^{\text{tot}} = 23.2$ ,  $\alpha_{\text{pz}} = 0.798$ , and  $z_{\text{pz};0} = 0.178$  (The LSST Dark Energy Science Collaboration et al. 2018). This total distribution is divided into five tomographic bins with equal number densities for each bin  $i$ ,  $\bar{n}_k^i = \bar{n}_k^{\text{tot}}/5$ . For shape noise, we expect  $\sigma_e = 0.26/\text{component}$ .

Given these source distributions, we compute the tomographic cosmic shear power spectra as a function of angular scale  $\ell$  as

$$C_\ell^{ij} = \int_{z_{\text{min}}}^{z_{\text{max}}} dz \frac{dV}{dz d\Omega} \frac{W_k^i(z)}{\chi^2} \frac{W_k^j(z)}{\chi^2} P(k, z), \quad (35)$$

where,  $i, j$  are the indices of tomographic bins,  $k = (\ell + 1/2)/\chi$ ,  $\chi$  is the comoving distance to redshift  $z$ , the integral is performed between  $z_{\text{min}} = 0$  and  $z_{\text{max}} = 3.0$ , and  $W_k^i(z)$  is the lensing efficiency given by:

$$W_k^i(z) = \frac{3H_0^2 \Omega_m}{2c^2} \frac{\chi}{a(\chi)} \int_\chi^\infty d\chi' n_k^i(z(\chi')) \frac{dz}{d\chi'} \frac{\chi' - \chi}{\chi'}. \quad (36)$$

Here,  $n_k^i$  represents the normalised redshift distribution of the source galaxies corresponding to the tomographic bin  $i$ .

Next, we calculate the covariance for the auto- and cross-correlations of cosmic shear power spectra for the five tomographic bins. In this work, we assume a Gaussian covariance, as described in Takada & Jain (2004). Note that we ignore the contributions non-Gaussian contributions arising from the trispectrum of matter fluctuations (Sato & Nishimichi 2013) and super-sample covariance (Krause & Eifler 2017). The super-sample covariance has been shown to be non-negligible for current and future-generation weak lensing surveys (Barreira et al. 2018). However, we remain conservative in our analysis choices and ignore their contributions here when quantifying the accuracy of our emulator.

To compare the effects of using different matter power spectra, for a LSST-like survey we need to be able to evaluate  $P(k, z)$  for approximately  $k \lesssim 10h^{-1} \text{Mpc}^{-1}$  and for  $z < 3$ . Given the coarse spacing of the snapshots of the `QUIOTE` simulation, unlike in Section 7.1, we choose not to use this as a benchmark as it is not clear that the interpolation required between redshifts would be accurate. Instead, we compare the predictions of different emulators, to see if their differences result in significantly different  $C_\ell$ ’s. Given the large discrepancies between `CLASS-HALOFIT` and `COSMOPOWER` when compared against `QUIOTE`

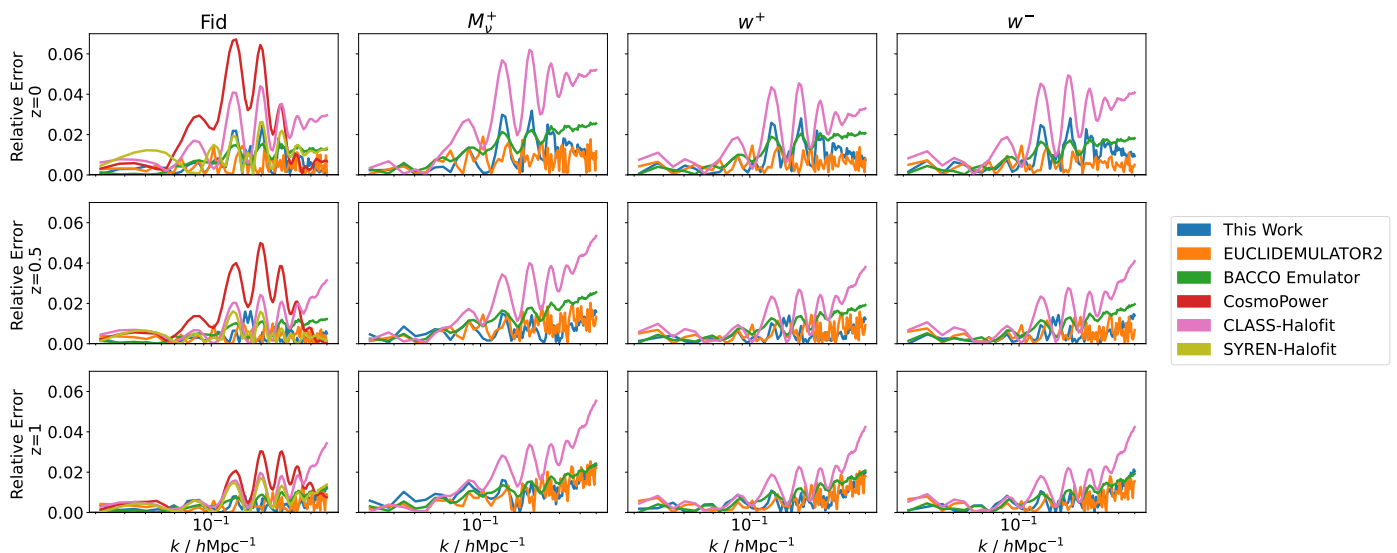


**Fig. 11.** Fractional error on the nonlinear power spectrum as a function of wavenumber,  $k$ , for various emulators at redshifts 0, 0.5 and 1. We apply each emulator only to test data that falls within its defined parameter space.

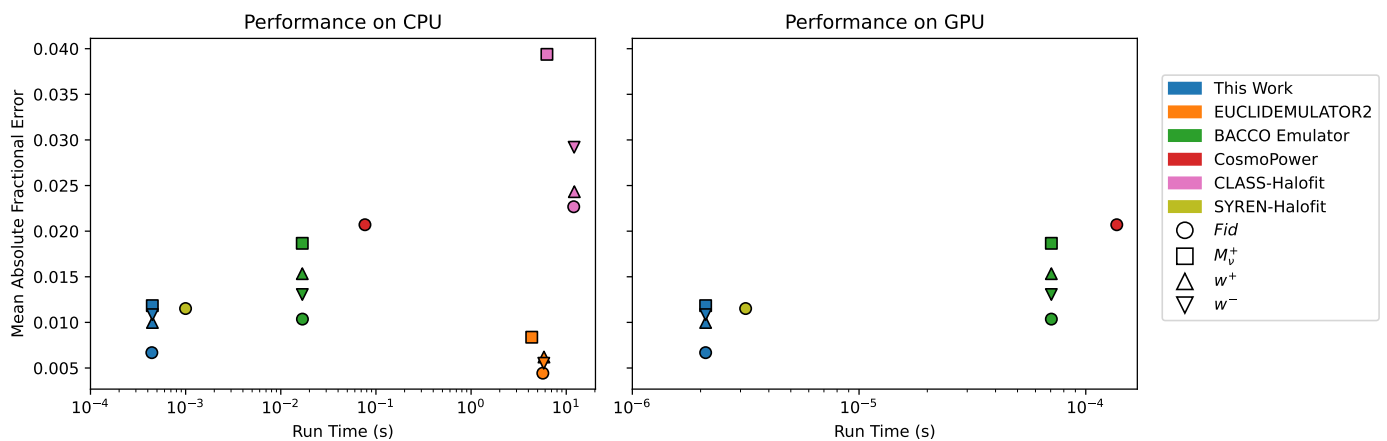


**Fig. 12.** Same as Fig. 10, but now comparing nonlinear emulators with the QUOTE simulations and averaging over  $k \in [0.02, 0.5] h \text{ Mpc}^{-1}$ .

(Fig. 11), we choose not to use these codes in our comparison, but consider those with approximately percent-level agreement: SYREN-HALOFIT, SYREN-NEW, BACCO and EUCLIDEMULATOR2. In fact, we cannot use BACCO since this is only trained up to  $z = 1.5$ , and thus cannot be used for higher-redshift surveys like LSST. For the three remaining codes, we assume the flat  $\Lambda$ CDM cosmology  $h = 0.6766$ ,  $\Omega_m = 0.3111$ ,  $\Omega_b = 0.0490$ ,  $\sigma_8 = 0.8102$ ,  $n_s = 0.9665$  (Planck Collaboration 2020) with massless neutrinos. To compute  $C_\ell$ , we evaluate  $P(k, z)$  on a  $128 \times 128$  two-dimensional grid, uniform in  $\log_{10} k$  and  $z$ , where  $5 \times 10^{-3} \leq k / h^{-1} \text{ Mpc}^{-1} \leq 9$  and  $0 < z < 3$ , which we use to numerically perform the integral Eq. (35).

The resulting  $C_\ell$ 's are plotted in Fig. 14, where we plot the ratio between the predictions from different emulators and that of EUCLIDEMULATOR2, for  $\ell < 4 \times 10^4$ . For reference, we plot the expected measured errors for Y1 and Y6 in bands. Qualitatively, we see that the differences between the predictions are always within the  $1\sigma$  band for both Y1 and Y6 for these angular scales, indicating that the percent-level disagreement for  $P(k)$  does not lead to significant differences on  $C_\ell$ . To estimate the range of angular scales for which the emulators do not yield significantly different results, we compute the total  $\Delta\chi^2$  between EUCLIDEMULATOR2 and the symbolic emulators when including all scales up

to some maximum  $\ell < \ell_{\max}$ . To ensure that this  $\Delta\chi^2$  remains less than unity, for SYREN-NEW one would have to use  $\ell_{\max} = 2000$  for Y1 data and  $\ell_{\max} = 1000$  for Y6, as indicated by the vertical lines in Fig. 14. We note that a full cosmological inference is required to quantify the impact of these  $\Delta\chi^2$  on the parameter biases which will depend on specific analysis choices and observational systematics, and is outside the scope of this study.<sup>3</sup>

On small scales, the effects of baryonic effects (e.g. astrophysical feedback from AGNs) and intrinsic alignments on the lensing power spectra are expected to be significant and which are poorly understood (e.g. see Krause et al. (2021) and references therein).<sup>4</sup> To estimate their importance, we use the halo model-based formalism, HMCODE (Mead et al. 2021), developed to capture the impact of baryonic feedback using an effective  $T_{\text{AGN}}$  parameter which controls the energy output from AGNs.

<sup>3</sup> However, as the residuals between our emulators and EUCLIDEMULATOR2 have a complicated shape, we expect a negligible impact on the  $S_8$  parameter that weak lensing mainly constrains (Jain & Seljak 1997) and is sensitive to the scale-independent amplitude of the power spectrum.

<sup>4</sup> Note that the Dark Energy Survey uses a range of scale-cuts corresponding to approximately  $\ell \lesssim 500$  (Doux et al. 2022) to mitigate these effects, which is much stricter than our  $\ell_{\max}$ .

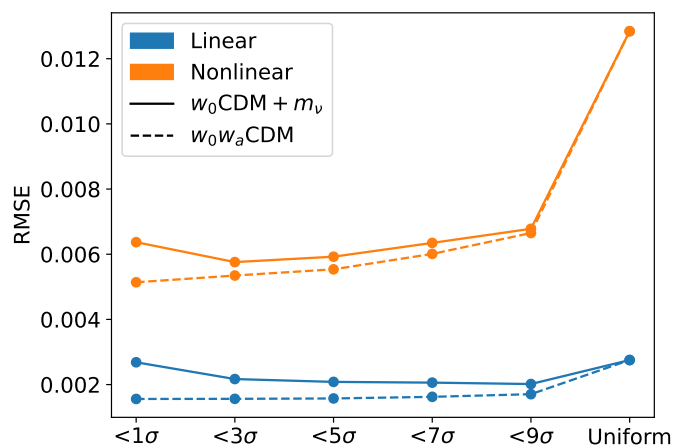


**Fig. 13.** Distribution of errors of the linear (blue) and nonlinear (orange) emulator as a function of distance from the best-fit model in the  $w_0w_a\text{CDM}$  subspace (dashed lines) and the  $w_0\text{CDM}+m_\nu$  subspace (solid lines). The  $x$ -axis represents the maximum  $\sigma$  value used for generating the test set. The "Uniform" case corresponds to generating test samples by uniformly sample parameters in the whole prior range.

In Fig. 14 we plot the ratio of  $C_\ell$  between the `HMCODE` predictions, when either excluding or including baryonic effects, where we choose an AGN temperature  $T_{\text{AGN}} = 10^8$  K as expected from various hydrodynamical simulations (Le Brun et al. 2017; McCarthy et al. 2018). We see that this ratio is much larger than the differences between the dark-matter-only emulators, and thus conclude that the dominant source of uncertainty when used in a weak lensing analysis is not due to the choice of emulator, but due to baryonic effects. As such, we advocate for the use of SYREN-NEW in such an analysis, given its speed and accuracy compared to other emulators (Fig. 12).

## 8. Conclusion

With current and future surveys poised to probe the mass of neutrinos and the nature of dark energy, rapid and accurate predictions of their effects on the linear and nonlinear evolution of matter in the Universe is essential. In this paper we have used symbolic regression to obtain analytic approximations to the linear and nonlinear matter power spectra as a function of redshift and cosmology in the presence of massive neutrinos and dynamical dark energy.

We obtained a succinct correction to previous symbolic approximations to the linear matter power spectrum which is accurate to within 0.3% across a wide range of cosmologies yet is  $3 \times 10^4$  times faster than using a Boltzmann code when both are run on a CPU. A further factor of 200 speed-up is possible when running on a GPU. Similarly, we produced a formula to compute the derived parameter  $\sigma_8$  as a function of  $A_s$  and other cosmological parameters, which does not require one to obtain or integrate the linear power spectrum, and is accurate to 0.1%. Analogous to `HALOFIT`, we found a fitting formula to predict the nonlinear matter power spectrum given the linear one, redshift and cosmological parameters. This approximation matches the predictions of `EUCLIDEMULATOR2` (Euclid Collaboration et al. 2021) to within 1.3% across a broad range of parameter space, redshift and wavenumbers, which is comparable to the level of discrepancy between different numerical emulators. The error is halved when considering cosmologies within the  $9\sigma$  region of current cosmological constraints (Alam et al. 2021), so we have sub-

percent agreement for cosmologies of physical interest. We find that the difference does not lead to significantly different predictions for modern, complex, multi-redshift bin, tomographic weak lensing surveys. We validated these predictions against  $N$ -body simulations, finding similar accuracy to numerical emulators while being over an order of magnitude faster, both on a CPU and GPU.

Unlike approaches such as `HMCODE`, our `HALOFIT`-like procedure does not include the effects of baryonic feedback, which become important on the smallest scales considered in this work. Future work should therefore be dedicated to obtaining baryonic corrections to our approximations so that one can marginalise over or infer these effects in cosmological analyses. We also note that here, as in Bartlett et al. (2024b), we chose to fit our models to the predictions of numerical emulators, which were themselves trained on  $N$ -body simulations since this provided an inexpensive method for producing power spectra. There is no fundamental reason to do this, and indeed one could limit the performance of the symbolic expression if the numerical emulator were not sufficiently accurate. As such, in future work it may be desirable to directly fit the symbolic models to simulations rather than use an intermediary numerical emulator.

Symbolic methods continue to demonstrate an ability to produce fitting formulae that are significantly faster to evaluate than numerical approaches without being less accurate. Such formulae are interpretable, and the correct limiting behaviour may readily be enforced. These advantages, coupled with the lack of reliance on particular programming languages or packages, will make symbolic methods valuable for a range of emulation tasks in astrophysics and cosmology.

## Acknowledgements

We thank Marco Bonici, Lukas Kammerer and Gabriel Kronberger for useful comments and suggestions. CS is supported by the National SKA Program of China (grant No. 2020SKA0110401) and NSFC (grant No. 11821303). DJB and SP are supported by the Simons Collaboration on "Learning the Universe." BDW acknowledges the DIM-ORIGINES-2023, *Infinity Next* grant. HD is supported by a Royal Society University Research Fellowship (grant no. 211046). PGF acknowledges STFC and the Beecroft Trust. This work has made use of the Infinity Cluster hosted by Institut d'Astrophysique de Paris; we thank Stephane Rouberol for running this cluster smoothly for us. Some of the computations reported in this paper were performed using resources made available by the Flatiron Institute. The Flatiron Institute is supported by the Simons Foundation.

For the purposes of open access, the authors have applied a Creative Commons Attribution (CC BY) licence to any Author Accepted Manuscript version arising.

The data underlying this article will be shared on reasonable request to the corresponding authors. We provide implementations of our emulators at [https://github.com/DeaglanBartlett/symbolic\\_pofk](https://github.com/DeaglanBartlett/symbolic_pofk).

## References

- AbdusSalam, S., Abel, S., & Crispim Romao, M. 2024, arXiv e-prints, arXiv:2405.18471
- Ahmed, S. N., Anthony, A. E., Beier, E. W., et al. 2004, Phys. Rev. Lett., 92, 181301
- Akeson, R., Armus, L., Bachelet, E., et al. 2019, arXiv e-prints, arXiv:1902.05569
- Alam, S., Aubert, M., Avila, S., et al. 2021, Physical Review D, 103
- Angulo, R. E., Zennaro, M., Contreras, S., et al. 2021, MNRAS, 507, 5869

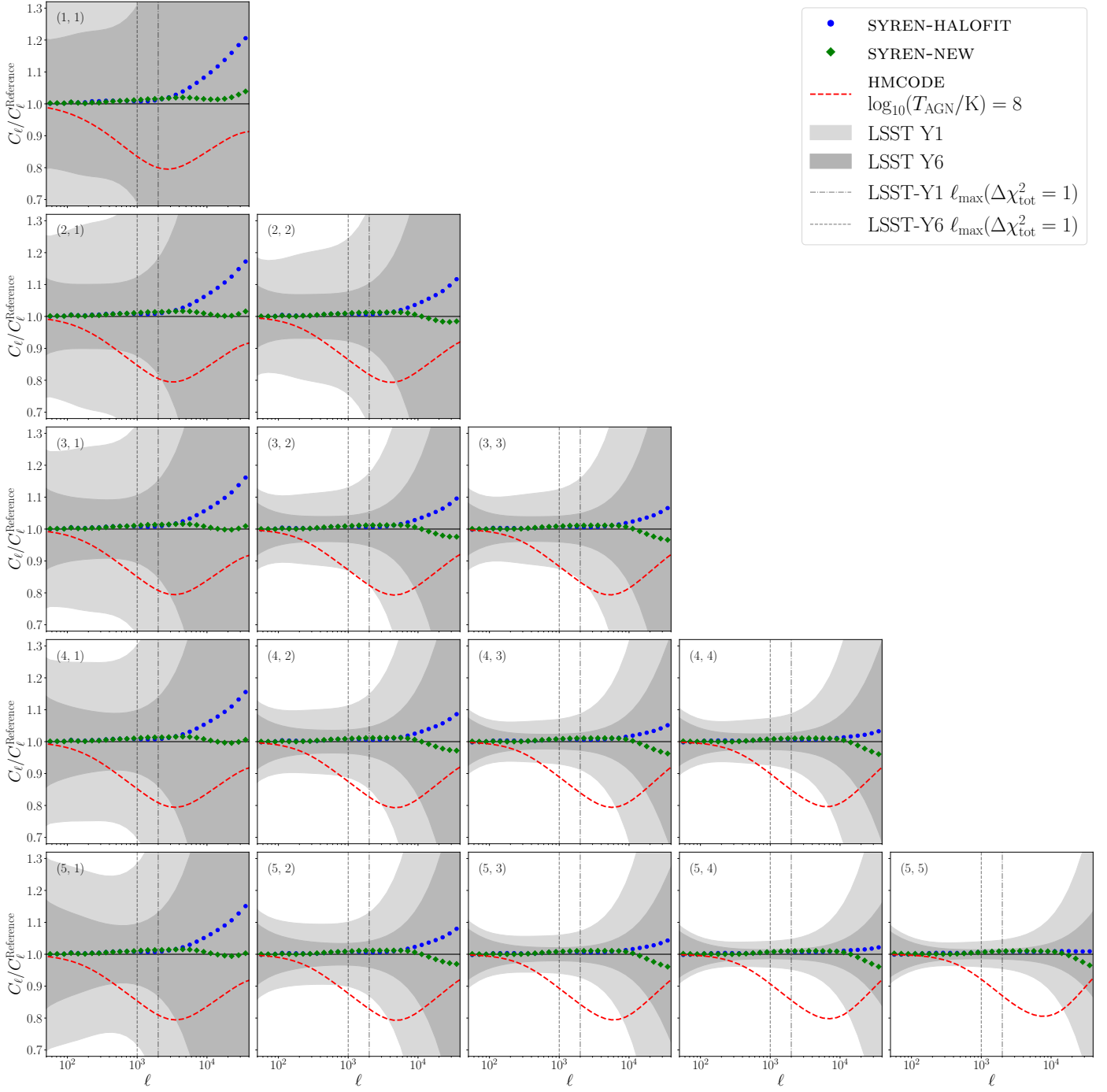


**Fig. 14.** Ratio of shear power spectra,  $C_\ell$  (Eq. (35)), computed with SYREN-HALOFIT and SYREN-NEW compared to that computed with EUCLIDEMULATOR2 for LSST. The light grey bands indicate the expected uncertainty for year 1 (Y1), whereas the dark bands are for year 6 (Y6). The numbers in the top left of each panel indicate the redshift bins between which we compute the  $C_\ell$ 's, such that the diagonal panels are auto-spectra and the off-diagonal ones are cross-spectra. To indicate the importance of baryonic effects, in red we plot the ratio of the HMCODE prediction in the presence of baryons (with  $\log_{10}(T_{\text{AGN}} / \text{K}) = 8$ ) to the dark-matter-only HMCODE prediction. With vertical lines, we show the scales for which the  $\Delta\chi_{\text{tot}}^2 = 1$  between our emulators and EUCLIDEMULATOR2 for full datavector for both LSST Y1 and Y6. The discrepancy between the emulators is small compared to the LSST errors and especially compared to the impact of baryonic effects for the angular scales shown.

Aricò, G., Angulo, R. E., & Zennaro, M. 2021 [arXiv:2104.14568]  
Bakx, T., Chisari, N. E., & Vlah, Z. 2024, arXiv e-prints, arXiv:2407.04660  
Bardeen, J. M., Bond, J. R., Kaiser, N., & Szalay, A. S. 1986, ApJ, 304, 15  
Barreira, A., Krause, E., & Schmidt, F. 2018, Journal of Cosmology and Astroparticle Physics, 2018, 015–015  
Bartlett, D. J., Desmond, H., & Ferreira, P. G. 2023, in The Genetic and Evolutionary Computation Conference 2023  
Bartlett, D. J., Desmond, H., & Ferreira, P. G. 2024, IEEE Transactions on Evolutionary Computation, 28, 950  
Bartlett, D. J., Kammerer, L., Kronberger, G., et al. 2024a, A&A, 686, A209

Bartlett, D. J., Wandelt, B. D., Zennaro, M., Ferreira, P. G., & Desmond, H. 2024b, A&A, 686, A150  
Bayer, A. E., Banerjee, A., & Seljak, U. 2022, Phys. Rev. D, 105, 123510  
Bayron Orjuela-Quintana, J., Sapone, D., & Nesseris, S. 2024, arXiv e-prints, arXiv:2407.16640  
Becker-Szendy, R., Bratton, C. B., Casper, D., et al. 1992, Phys. Rev. D, 46, 3720  
Bird, S., Viel, M., & Haehnelt, M. G. 2012, MNRAS, 420, 2551  
Blas, D., Lesgourgues, J., & Tram, T. 2011, J. Cosmology Astropart. Phys., 2011, 034



- Bond, J. R., Efstathiou, G., & Silk, J. 1980, *Phys. Rev. Lett.*, 45, 1980
- Burlacu, B. 2023, in *Proceedings of the Companion Conference on Genetic and Evolutionary Computation, GECCO '23 Companion* (New York, NY, USA: Association for Computing Machinery), 2412–2419
- Burlacu, B., Kronberger, G., & Kommenda, M. 2020, in *Proceedings of the 2020 Genetic and Evolutionary Computation Conference Companion, GECCO '20* (New York, NY, USA: Association for Computing Machinery), 1562–1570
- Carroll, S. M., Press, W. H., & Turner, E. L. 1992, *ARA&A*, 30, 499
- Cava, W. G. L., Orzechowski, P., Burlacu, B., et al. 2021, *CoRR*, abs/2107.14351 [2107.14351]
- Chevallier, M. & Polarski, D. 2001, *Int. J. Mod. Phys. D*, 10, 213
- Cooray, A. & Sheth, R. 2002, *Phys. Rep.*, 372, 1
- Cranmer, M., Sanchez Gonzalez, A., Battaglia, P., et al. 2020, *Discovering Symbolic Models from Deep Learning with Inductive Biases*
- David, E. 1989, *Genetic Algorithms in Search, Optimization and Machine Learning* (Addison-Wesley)
- DESI Collaboration, Adame, A. G., Aguilar, J., et al. 2024, arXiv e-prints, arXiv:2404.03002
- DESI Collaboration, Aghamousa, A., Aguilar, J., et al. 2016, arXiv e-prints, arXiv:1611.00036
- Doux, C., Jain, B., Zeurher, D., et al. 2022, *MNRAS*, 515, 1942
- Eisenstein, D. J. & Hu, W. 1998, *ApJ*, 496, 605
- Eisenstein, D. J. & Hu, W. 1999, *ApJ*, 511, 5
- Euclid Collaboration, Knabenhans, M., Stadel, J., et al. 2019, *MNRAS*, 484, 5509
- Euclid Collaboration et al. 2021, *MNRAS*, 505, 2840
- Fendt, W. A. & Wandelt, B. D. 2007a, arXiv e-prints, arXiv:0712.0194
- Fendt, W. A. & Wandelt, B. D. 2007b, *ApJ*, 654, 2
- Fukuda, Y., Hayakawa, T., Ichihara, E., et al. 1998a, *Phys. Rev. Lett.*, 81, 1158
- Fukuda, Y., Hayakawa, T., Ichihara, E., et al. 1998b, *Phys. Rev. Lett.*, 81, 1562
- Hahn, O., List, F., & Porqueres, N. 2024, *J. Cosmology Astropart. Phys.*, 2024, 063
- Haupt, R. & Haupt, S. 2004, *Practical genetic algorithms*, 2nd edn. (Wiley)
- Heitmann, K., Higdon, D., White, M., et al. 2009, *ApJ*, 705, 156
- Heitmann, K., Lawrence, E., Kwan, J., Habib, S., & Higdon, D. 2014, *ApJ*, 780, 111
- Hu, W. & Eisenstein, D. J. 1998, *ApJ*, 498, 497
- Jain, B. & Seljak, U. 1997, *ApJ*, 484, 560
- Kolb, E. W. & Turner, M. S. 1990, *The Early Universe*, Vol. 69
- Kommenda, M., Burlacu, B., Kronberger, G., & Affenzeller, M. 2020, *Genetic Programming and Evolvable Machines*, 21, 471–501
- Krause, E. & Eifler, T. 2017, *MNRAS*, 470, 2100
- Krause, E., Fang, X., Pandey, S., et al. 2021, arXiv e-prints, arXiv:2105.13548
- Kronberger, G., Burlacu, B., Kommenda, M., Winkler, S. M., & Affenzeller, M. 2024, *Symbolic Regression* (Chapman & Hall / CRC Press)
- Lahav, O., Lilje, P. B., Primack, J. R., & Rees, M. J. 1991, *MNRAS*, 251, 128
- Laumanns, M., Thiele, L., Deb, K., & Zitzler, E. 2002, *Evol. Comput.*, 10, 263–282
- Laureijs, R., Amiaux, J., Arduini, S., et al. 2011, arXiv e-prints, arXiv:1110.3193
- Lawrence, E., Heitmann, K., Kwan, J., et al. 2017, *ApJ*, 847, 50
- Le Brun, A. M. C., McCarthy, I. G., Schaye, J., & Ponman, T. J. 2017, *MNRAS*, 466, 4442
- Lesgourgues, J. & Pastor, S. 2006, *Phys. Rep.*, 429, 307
- Levenberg, K. 1944, *Quarterly of Applied Mathematics*, 2, 164
- Lewis, A., Challinor, A., & Lasenby, A. 2000, *ApJ*, 538, 473
- Linder, E. V. 2003, *Phys. Rev. Lett.*, 90, 091301
- LSST Science Collaboration, Abell, P. A., Allison, J., et al. 2009, arXiv e-prints, arXiv:0912.0201
- Ma, C.-P. & Fry, J. N. 2000, *ApJ*, 543, 503
- Marquardt, D. W. 1963, *Journal of the Society for Industrial and Applied Mathematics*, 11, 431
- Mather, J. C., Fixsen, D. J., Shafer, R. A., Mosier, C., & Wilkinson, D. T. 1999, *ApJ*, 512, 511
- McCarthy, I. G., Bird, S., Schaye, J., et al. 2018, *MNRAS*, 476, 2999
- Mead, A. J., Brieden, S., Tröster, T., & Heymans, C. 2021, *MNRAS*, 502, 1401
- Mead, A. J., Heymans, C., Lombriser, L., et al. 2016, *MNRAS*, 459, 1468
- Mead, A. J., Peacock, J. A., Heymans, C., Joudaki, S., & Heavens, A. F. 2015, *MNRAS*, 454, 1958
- Mootoovaloo, A., Jaffe, A. H., Heavens, A. F., & Leclercq, F. 2022, *Astronomy and Computing*, 38, 100508
- Nishimichi, T., Takada, M., Takahashi, R., et al. 2019, *ApJ*, 884, 29
- Orjuela-Quintana, J. B., Nesseris, S., & Sapone, D. 2024, *Phys. Rev. D*, 109, 063511
- Planck Collaboration. 2020, *A&A*, 641, A6
- Russeil, E., de Franca, F. O., Malanchev, K., et al. 2024, in *Proceedings of the Genetic and Evolutionary Computation Conference, GECCO '24* (New York, NY, USA: Association for Computing Machinery), 961–970
- Sato, M. & Nishimichi, T. 2013, *Physical Review D*, 87
- Seljak, U. 2000, *MNRAS*, 318, 203
- Smith, R. E. & Angulo, R. E. 2019, *MNRAS*, 486, 1448
- Smith, R. E., Peacock, J. A., Jenkins, A., et al. 2003, *MNRAS*, 341, 1311
- Springel, V. 2005, *MNRAS*, 364, 1105
- Spurio Mancini, A., Piras, D., Alsing, J., Joachimi, B., & Hobson, M. P. 2022, *MNRAS*, 511, 1771
- Takada, M. & Jain, B. 2004, *MNRAS*, 348, 897
- Takahashi, R., Sato, M., Nishimichi, T., Taruya, A., & Oguri, M. 2012, *ApJ*, 761, 152
- Taylor, P. L., Kitching, T. D., & McEwen, J. D. 2018, *Phys. Rev. D*, 98, 043532
- The LSST Dark Energy Science Collaboration, Mandelbaum, R., Eifler, T., et al. 2018, arXiv e-prints, arXiv:1809.01669
- Turing, A. M. 1950, *Mind*, LIX, 433
- Villaescusa-Navarro, F., Hahn, C., Massara, E., et al. 2020, *ApJS*, 250, 2
- Weinberg, D. H., Mortonson, M. J., Eisenstein, D. J., et al. 2013, *Phys. Rep.*, 530, 87
- Winther, H. A., Casas, S., Baldi, M., et al. 2019, *Phys. Rev. D*, 100, 123540
- Zennaro, M., Angulo, R. E., Pellejero-Ibáñez, M., et al. 2023, *MNRAS*, 524, 2407
- Zhai, Z., Tinker, J. L., Becker, M. R., et al. 2019, *ApJ*, 874, 95

## Appendix A: Most accurate analytic expression found for $\sigma_8$

Here, we present an analytical approximation for  $\sigma_8$  that, unlike Eq. (5) which attempts to balance accu-

racy and simplicity, is the most accurate one found. This is the model at length 89 in Fig. 1 and is given by

$$\begin{aligned} \frac{\sigma_8}{\sqrt{10^9 A_s}} &\approx \tilde{c}_0 (\Omega_m \tilde{c}_1 + (\tilde{c}_2 m_\nu - \tilde{c}_3 n_s + \log(\tilde{c}_4 h - \tilde{c}_5 m_\nu)) (\tilde{c}_6 h + \tilde{c}_7 m_\nu - \tilde{c}_8 n_s + 1)) (\tilde{c}_9 h - m_\nu) \\ &\times (\tilde{c}_{10} w_0 - \tilde{c}_{11} m_\nu - (\tilde{c}_{12} w_0 - \tilde{c}_{13} w_a - \log(\Omega_m \tilde{c}_{14})) (\Omega_m \tilde{c}_{15} + \tilde{c}_{16} w_0 + \tilde{c}_{17} w_a + \log(-\tilde{c}_{18} w_0 - \tilde{c}_{19} w_a)) \\ &- \log(\Omega_m \tilde{c}_{20} + \log(-\tilde{c}_{21} w_0 - \tilde{c}_{22} w_a)) + \log(-\tilde{c}_{23} w_0 - \tilde{c}_{24} w_a)) \\ &\times (\tilde{c}_{25} m_\nu - \sqrt{\Omega_b} \tilde{c}_{26} - \Omega_b \tilde{c}_{27} + \Omega_m \tilde{c}_{28} - \tilde{c}_{29} h + 1 + (\Omega_b \tilde{c}_{30} - \tilde{c}_{31} h - \log(\Omega_m \tilde{c}_{32})) (\Omega_m \tilde{c}_{33} - \tilde{c}_{34} h - \tilde{c}_{35} m_\nu - \tilde{c}_{36} n_s)), \quad (\text{A.1}) \end{aligned}$$

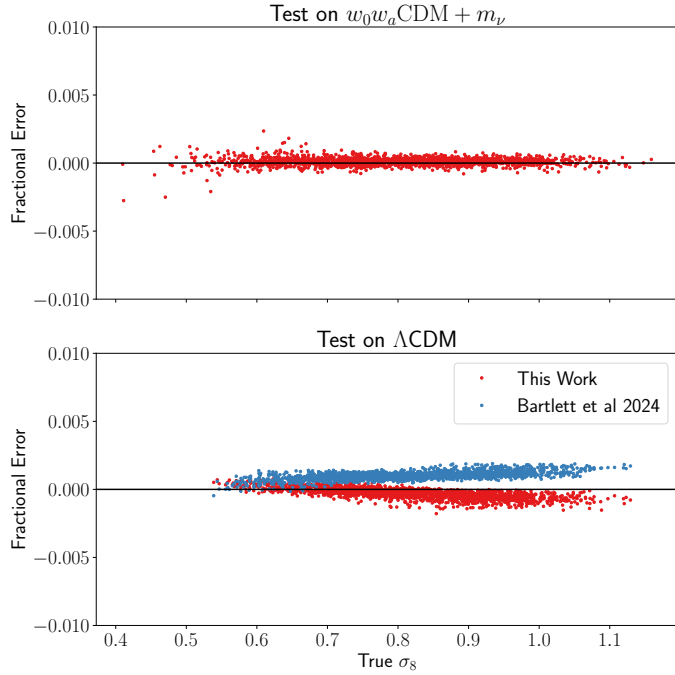


**Fig. A.1.** Fractional error on the  $\sigma_8$  prediction tested on  $w_0 w_a \text{CDM} + m_\nu$  (upper) and  $\Lambda \text{CDM}$  (bottom) models using the most accurate  $\sigma_8$  expression (Eq. (A.1)). For the  $\Lambda \text{CDM}$  case, we also compare the results of the emulator given here to that of Bartlett et al. (2024a).

where the parameters  $\tilde{c}$  are given in Table A.1. Although this form is rather long, we include it in case a more accurate conversion is required. We find that it has a root mean squared error on the  $w_0 w_a \text{CDM} + m_\nu$  and  $\Lambda \text{CDM}$  test sets of 0.02% and 0.04%, respectively. We plot the variation of this error with the true  $\sigma_8$  value in Fig. A.1. For the  $w_0 w_a \text{CDM} + m_\nu$  model, the errors are significantly smaller compared to those in Fig. 2, while for  $\Lambda \text{CDM}$ , our results show comparable performance to Bartlett et al. (2024a).

**Table A.1.** Best-fit parameters for  $\sigma_8$  given in Eq. (A.1).

Param.	Value	Param.	Value	Param.	Value
$\tilde{c}_0$	0.0246	$\tilde{c}_{13}$	0.5466	$\tilde{c}_{26}$	1.2991
$\tilde{c}_1$	2.1062	$\tilde{c}_{14}$	0.5519	$\tilde{c}_{27}$	4.1426
$\tilde{c}_2$	2.9355	$\tilde{c}_{15}$	0.3689	$\tilde{c}_{28}$	3.3055
$\tilde{c}_3$	0.7626	$\tilde{c}_{16}$	0.3261	$\tilde{c}_{29}$	0.5716
$\tilde{c}_4$	0.2962	$\tilde{c}_{17}$	0.2002	$\tilde{c}_{30}$	6.0094
$\tilde{c}_5$	0.5096	$\tilde{c}_{18}$	0.8892	$\tilde{c}_{31}$	1.9569
$\tilde{c}_6$	4.4025	$\tilde{c}_{19}$	0.4462	$\tilde{c}_{32}$	2.1477
$\tilde{c}_7$	3.6495	$\tilde{c}_{20}$	1.215	$\tilde{c}_{33}$	1.1902
$\tilde{c}_8$	0.4144	$\tilde{c}_{21}$	3.4829	$\tilde{c}_{34}$	0.128
$\tilde{c}_9$	0.8615	$\tilde{c}_{22}$	2.5852	$\tilde{c}_{35}$	0.6931
$\tilde{c}_{10}$	0.6188	$\tilde{c}_{23}$	0.0242	$\tilde{c}_{36}$	0.2661
$\tilde{c}_{11}$	0.1751	$\tilde{c}_{24}$	0.0051		
$\tilde{c}_{12}$	0.824	$\tilde{c}_{25}$	0.1614		